# PLOS ONE

RESEARCH ARTICLE

# Small extracellular vesicle-encapsulated miR-181b-5p, miR-222-3p and let-7a-5p: Next generation plasma biopsy-based diagnostic biomarkers for inflammatory breast cancer

Sarah Hamdy Ahmed[1], Nancy A. Espinoza-Sánchez[2,3], Ahmed El-Damen[4], Sarah Atef Fahim[5], Mohamed A. Badawy[6], Burkhard Greve[3], Mohamed El-Shinawi[7,8], Martin Götte[2☯], Sherif Abdelaziz Ibrahim[4☯]*

1 Biotechnology/Biomolecular Chemistry Program, Chemistry Department, Faculty of Science, Cairo University, Giza, Egypt, 2 Department of Gynecology and Obstetrics, Münster University Hospital, Münster, Germany, 3 Department of Radiotherapy–Radiooncology, University Hospital Münster, Münster, Germany, 4 Department of Zoology, Faculty of Science, Cairo University, Giza, Egypt, 5 Biochemistry Program, Chemistry Department, Faculty of Science, Cairo University, Giza, Egypt, 6 Chemistry Department, Faculty of Science, Cairo University, Giza, Egypt, 7 Galala University, Suez, Egypt, 8 Department of General Surgery, Faculty of Medicine, Ain Shams University, Cairo, Egypt

☯ These authors contributed equally to this work.
* isherif3380@gmail.com, isherif@sci.cu.edu.eg

## Abstract

Inflammatory breast cancer (IBC) is a rare, but aggressive entity of breast carcinoma with rapid dermal lymphatic invasion in young females. It is either poorly or misdiagnosed as mastitis because of the absence of a distinct lump. Small extracellular vesicles (sEVs) circulating in liquid biopsies are a novel class of minimally invasive diagnostic alternative to invasive tissue biopsies. They modulate cancer progression via shuttling their encapsulated cargo including microRNAs (miRNAs) into recipient cells to either trigger signaling or induce malignant transformation of targeted cells. Plasma sEVs < 200 nm were isolated using a modified cost-effective polyethylene glycol (PEG)-based precipitation method and compared to standard methods, namely ultracentrifugation and a commercial kit, where the successful isolation was verified by different approaches. We evaluated the expression levels of selected sEV-derived miR-181b-5p, miR-222-3p and let-7a-5p using quantitative real PCR (qPCR). Relative to non-IBC, our qPCR data showed that sEV-derived miR-181b-5p and miR-222-3p were significantly upregulated, whereas let-7a-5p was downregulated in IBC patients. Interestingly, receiver operating characteristic (ROC) curves analysis revealed that diagnostic accuracy of let-7a-5p alone was the highest for IBC with an area under curve (AUC) value of 0.9188, and when combined with miR-222-3p the AUC was improved to 0.973. Further, 38 hub genes were identified using bioinformatics analysis. Together, circulating sEV-derived miR-181b-5p, miR-222-3p and let-7a-5p serve as promising non-invasive diagnostic biomarkers for IBC.

## Introduction

Inflammatory breast cancer (IBC) is the most lethal locally advanced breast cancer variant [1]. It is a relatively infrequent aggressive form of cancer that grows within the dermal lymphatics of breast tissue. It accounts for 1 to 6% of breast cancer in western countries, while its incidence is as high as 10% within the middle East [2, 3]. Based on clinical statements, one-third of the affected breast is commonly associated with erythema, edema (orange-peel appearance) and warmness [2]. The 5- year overall survival rate of IBC is 55% shorter than that of non-inflammatory breast cancer (non-IBC), with a median survival of 2.9 to 3.8 years[4, 5]. Further, approximately 75% of IBC patients are pathologically diagnosed with lymph vascular tumor emboli, which accounts for strong metastatic behavior and poor prognosis [1]. IBC diagnosis is challenged by overlapping signs and symptoms of other diseases, and approximately 30% of newly diagnosed cases with distant metastases [6]. IBC rarity, aggressiveness and misdiagnosis resulted in delayed definition of an effective treatment [3]. The substantial pain and discomfort during collecting tissue biopsies at different time points, renders early noninvasive detection an urgent priority for better management of IBC patient's outcome.

Liquid biopsies are emerging as a fascinating minimally invasive alternative to gold standard sampling procedures. They permit easy sequential sampling for monitoring cancer recurrence, therapy response, or any tumor genomic changes in real time, thus saving costs, time and avoiding pain associated with invasive biopsies [7]. Eukaryotic cells release complex vesicular entities that were deemed to be junk cell debris for prolonged time. It wasn't until recent, that these were revealed to be tailor-made cell specific extracellular vesicles (EVs) [8]. The EVs circulating within liquid biopsies involve small (30–200 nm) and large (up to 1000 nm) bodies that are commonly classified according to their size and origin [9]. These nanovesicles promote and maintain cancer progression, cell-cell signaling, carcinogenesis, tumor microenvironment modulation and angiogenesis via shuttling their cargo into recipient cells [9]. EVs contain microRNAs (miRNAs), small posttranscriptional regulatory non-coding RNAs, which cleave either their target mRNA or suppress translation. miRNAs are widely used as reliable biomarkers; where their differential expression profile is accompanied by different pathological conditions [10]. Of note, free plasma circulating miRNAs were identified as biomarker candidates for breast cancer, however they were challenged by the enormous variations among clinical studies in respect to their selection and specificity to breast cancer. On the contrary, EVs-derived miRNAs are a more appealing choice for diagnostic and prognostic biomarkers and robust alternative for invasive tissue biopsies [11].

Several challenges for a quick and efficient EV isolation method are frequently reported [12]. Although ultracentrifugation is the most adopted isolation method in different studies, it is not applicable for clinical studies, where only limited volumes of samples are available. Further, laborious and extended time is needed as EV sedimentation efficiency decreases in biological fluids [13]. Additionally, repeated centrifugation cycles at higher speeds results in low sEVs yields compared to polyethylene glycol (PEG)-based isolation methods [13]. Commercially available kits are not only overpriced, but also co-isolate various larger EVs [14]. Conversely, the cost-effective PEG could be adapted in different approaches to isolate functional sEVs from liquid biopsies. Different studies have demonstrated that simple adaption of virus enrichment methods could be efficient and reproducible in enriching various EVs [15–17]. In particular, PEG of different molecular weights is a non-toxic and far less expensive precipitant for EVs than commercial polymer-based kits [18].

Hence, in the present study, we isolated sEVs through a modified PEG-based method, analyzed the expression pattern of five selected miRNAs as sEV cargo and assessed their use as alternative minimally invasive diagnostic biomarker candidates for IBC.

## Materials and methods

### Human subjects and study design

All liquid biopsy collection and preparation procedures were approved by the Institutional Review Board (IRB0006379) of Ain Shams University, Cairo, Egypt. Following the Declaration of Helsinki, all participants signed an informed consent to be enrolled in this investigation. Patients included were neither pregnant nor issued with bloodborne or autoimmune disease, while healthy subjects had no oncologic history. This prospective case-control study included 77 women; 57 were diagnosed with breast cancer (34 non-IBC and 23 IBC), while 20 were healthy volunteers used as control group. This study followed two consecutive phases: procedure optimization (n = 12) and biomarker screening phase (n = 77). Peripheral blood was collected on the same day of the curative surgery in EDTA coated vacutainers (BD Bioscience, CA, USA) and centrifuged for 10 min at 1,500 g to isolate plasma. All clinicopathological data including age, tumor size, tumor grade, lymphovascular invasion, lymph node metastasis, estrogen receptor (ER) status, progesterone receptor (PR) status, and human epidermal growth receptor 2 (HER-2) were collected from the clinical and pathological records.

### sEVs enrichment

For sEVs isolation procedure optimization phase, twelve plasma samples were pooled (0.25 µl / sample) and differentially centrifuged twice; at 2000 g for 10 min and 10,000 g for 30 min to eliminate cellular debris and non-EV bodies, respectively, as depicted in Fig 1A. Pooled samples were subsequently ultra-filtrated with 0.22µm syringe filters, diluted with PBS to minimize plasma viscosity, which may lead to density gradients formation that may hinder subsequent EVs pelleting, and further processing through different approaches, including single polyethylene glycol treatment (SPEGT), double polyethylene glycol treatment (DPEGT), ultracentrifugation and the miRCURY Exosome Plasma Kit (Fig 1B). Finally, EVs were either processed directly for miRNA and protein extraction or kept at -80˚C prior to analysis.

### Single Polyethylene Glycol Treatment (SPEGT)

Firstly, polyethylene glycol (PEG) precipitation involved dissolving 20 grams of PEG6000 (Sigma, Cat#81260, MO, USA) in 50 mL nuclease-free water (Qiagen, Cat#129115, Hilden, Germany) to prepare 40% (w/v) sterile PEG6000 stock. This homogenous liquid stock was afterward ultra-filtrated with a 0.22µm syringe filter to exclude any contaminating particles, diluted to reach the final 5, 8, 10, 12, and 15% concentrations, and eventually added to differentially centrifuged clinical plasma pooled samples. In SPEGT, plasma pooled samples (n = 12) were mixed with the different PEG concentrations at 4˚C overnight. Afterward, samples were centrifuged at 10,000 g for 1h. Then, the supernatant was aspirated and the sEVs pellet was washed with 1X PBS (Fig 1**B**1).

### Double Polyethylene Glycol Treatment (DPEGT)

The same previous liquid stock preparation and steps were followed and the initial 10k EV pellet was re-washed with 1X PBS. Additionally, 0.25 µg/µl Proteinase K (Thermo Scientific, Cat#EO0491, MA, USA) was added for 20 min at 37˚C to reduce the extensive loads of circulating EVs masking proteins (e.g., albumin and lipoproteins) and followed by reprecipitating the sEV pellet using different PEG concentrations (Fig 1B2).
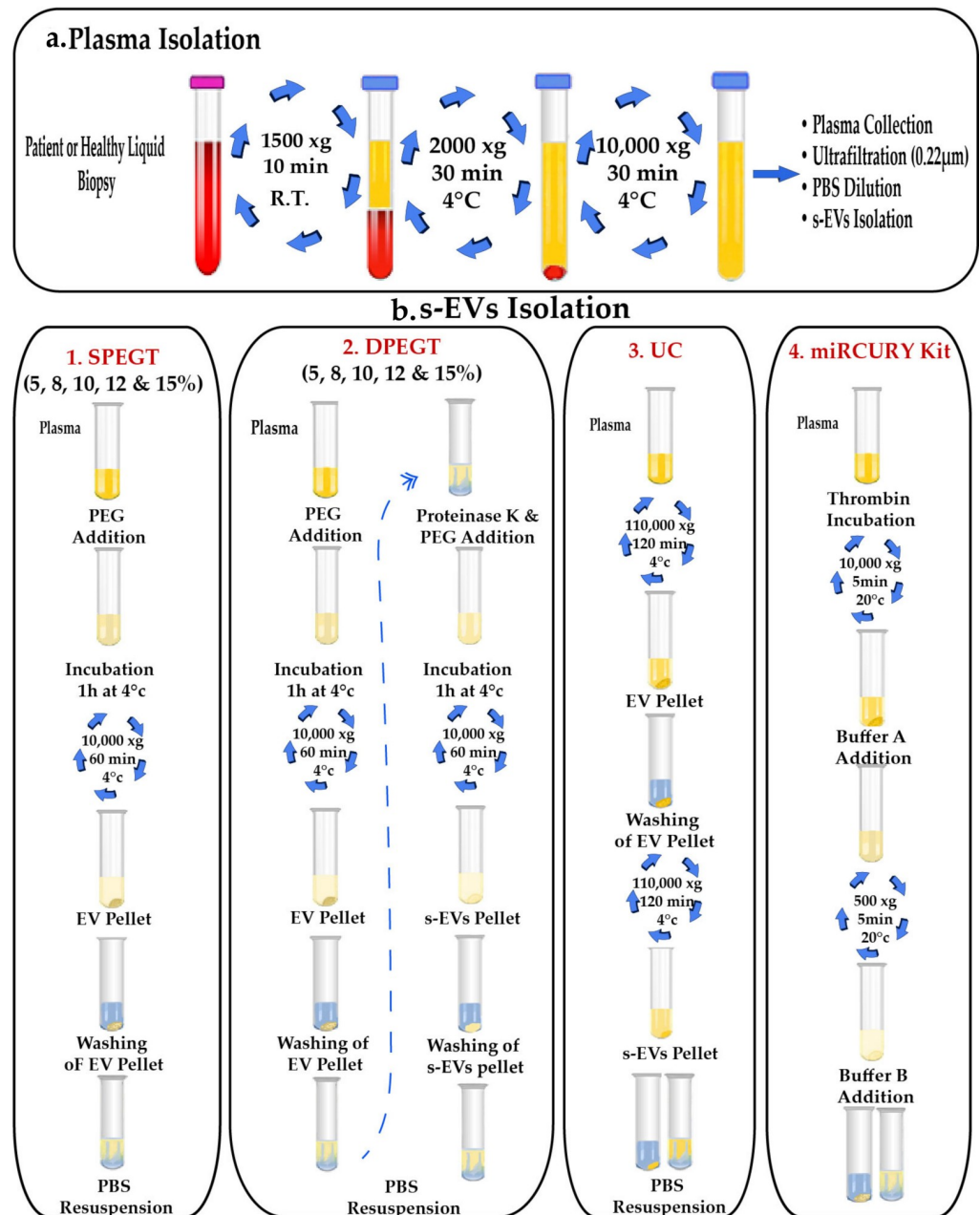
**Fig 1. Schematic illustration of isolation procedures for sEVs.** (a) Blood processing and plasma isolation. (b) Detailed steps of sEVs isolation using single PEG6000 treatment (SPEGT), double PEG6000 treatment (DPEGT), ultracentrifugation (UC) and miRCURY kit. The PEG incubation period could optionally range from 1 to 24 hrs.

https://doi.org/10.1371/journal.pone.0250642.g001

## Ultracentrifugation (UC)

The UC procedure was optimized following the protocol of Kim *et al.* [19], with some modifications. Pooled plasma biopsies (n = 6) were centrifuged as mentioned before, diluted with 1X PBS, and carefully transferred to ultra-clear centrifuge tubes (Thermo Scientific). EVs were precipitated at 110,000 g for 2h at 4°C using Sorval MTX 150 micro-ultracentrifuge (Thermo Scientific, S50-A 2238 rotor). The initial 110k EV pellets were subsequently washed with 1X

PBS, filtered with a 0.22μm filter (Millipore), and re-centrifuged at 110,000 g for 2h at 4˚C. Finally, the final 110k sEV pellet was resuspended in 250 μL PBS (Fig 1B3).

## MiRCURY exosome plasma kit

Pooled plasma (n = 12) was processed according to the manufacturer's instructions of the miRCURY Exosome Plasma Kit (Qiagen, Cat#76603). In brief, 6 μL of 500 U/mL Thrombin was added to 0.6 mL liquid biopsy, incubated for 5 min at 25˚C, and centrifuged at 10,000 g for 5 min. The supernatant was gently mixed with the precipitation buffer A, incubated overnight at 4˚C, and the resuspension buffer B was added to the 0.5k EV pellet (Fig 1B4).

## sEVs characterization

According to the International Society of Extracellular Vesicles (ISEV) guidelines, at least three different techniques should be used to characterize EVs [20]. Therefore, dynamic light scattering (DLS), transmission electron microscopy (TEM) and Western blot analysis were used in this study.

## Dynamic Light Scattering (DLS)

sEVs (10 μL) from the four procedures were diluted in 1 mL sterile MilliQ pure water or PBS and mixed thoroughly to attain an equally distributed homogenous solution. The size and Poly Dispersity Index (PDI) of sEVs were measured via Malvern Zetasizer Nano ZS90 (ZEN 3600, Malvern Instruments, Worcestershire, UK) (available at Cairo University Research Park, Faculty of Agriculture) equipped with a 633-nm He-Ne laser. Data were analyzed using Malvern zeta sizer software version 7.12 at a position of 4.65 mm from the cuvette wall with an automatic attenuator at a controlled temperature of 25˚C. Each sample was subjected to 15 runs of 10 s and three replicates. The adapted material refractive index (RI) was 1.37 while dispersant RI was 1.33 for water and 1.34 for PBS, the viscosity was 0.89 cP for water and 1.02 cP for PBS [21].

## Transmission Electron Microscopy (TEM)

The size and morphology of sEVs were resolved by TEM. Briefly, 20–50 μL drop of the suspension was loaded onto a 200-mesh copper-coated grid for 15–30 min in a dry environment, fixed with 2% glutaraldehyde for 15 min, and the grids were rinsed four times in 100 μL MilliQ water. sEVs were stained for 10 min via a 30 μL drop of 2.5% uranyl acetate and excess liquid was removed using filter paper. Imaging was performed at 120 kV with JEOL-JEM 1200EX II Transmission Electron Microscope (Tokyo, Japan) (available at Cairo University Research Park, Faculty of Agriculture). Images were captured using a 4k*4k image resolution Eagle CCD camera.

## Protein quantification

The protein concentration of the isolated fractions was quantified using a BCA protein assay kit (Pierce, Thermo Scientific, Cat#23227) according to the manufacturer's protocol. Briefly, bovine serum albumin (BSA) standards and samples were pipetted (25 μL/well) into the 96-microplate and mixed thoroughly with 200 μL of working reagent on a plate shaker for 30 seconds. After incubation at 37˚C for 30 min, the absorbance was measured at 562 nm using Nanoquant Tecan Infinite PRO 200 (Tecan, Switzerland), and BSA standard curve was used to determine the sample protein concentration.

## Western blot

Equal sample volumes (16 μL) were lysed with 4 μL of 5X reducing sample buffer (1 M Tris-HCl (pH 6.8), 30% glycerol, 6% SDS, 3% 2-mercaptoethanol, 0.005% bromophenol blue) and boiled at 95˚C for 5 min. Pooled samples (n = 12) were separated onto a 10% SDS-PAGE and electro-transferred onto a nitrocellulose membrane (Amersham, UK). Membranes were blocked with 5% non-fat skimmed milk in TBST, followed by overnight incubation with the following primary exosomes specific antibodies diluted at 1:500 HSP70 (sc-24, Santa Cruz, TX, USA), CD63 (Sc-5275, Santa Cruz), GM130 (P-20, sc-16268, Santa Cruz), Alix (sc-53540, Santa Cruz), and GAPDH (sc-20357, Santa Cruz). Subsequently, horseradish peroxidase (HRP)-conjugated anti-mouse secondary antibody (Sigma Aldrich) diluted at 1:2500 was applied for 1h. Finally, membranes were washed thrice with TBST, and the enhanced chemiluminescent (ECL) HRP substrate (Thermo Scientific, Waltham, USA) was used for signal development. Chemiluminescence was detected using the UVP Biospectrum Imaging System and Image Acquisition and Analysis Software (Analytik Jena, Cambridge, UK).

## RNA extraction

Total RNA extraction from sEVs was performed using Qiazol lysis reagent (Qiagen, 79306) following the manufacturer's protocol. All fractions were pre-incubated with RNase A (10 mg/ml) (Thermo Scientific, Cat#EN0531) at 37˚C for 40 min to eliminate cross-contamination with free circulating RNA before RNA extraction. Briefly, 350 μL sample input was mixed with three volumes of Qiazol (Qiagen), centrifuged at 12,000 g for 10 min at 4˚C to remove the fatty layer particulates, and 1.5 μL of the synthetic *Caenorhabditis elegans* cel-miR-39 (MS00019789, Qiagen) was spiked into the lysate. Afterward, 200 μL chloroform was mixed with the homogenate to separate the aqueous phase and an equal volume of isopropanol along with 0.8 μg/μL of carrier MS2 RNA (Roche Diagnostics GmbH, Mannheim, Germany) were added. RNA was washed with 70% ethanol and eluted in 20 μL RNase free water, then concentrations at 230, 260 and, 280 nm were estimated using Nanoquant Tecan Infinite PRO 200 spectrophotometer (Tecan, Switzerland). RNA samples were processed directly for cDNA synthesis, then stored at -20˚C till RT-qPCR analysis, where miRNA expression levels were assessed to compare efficiency of sEVs isolation methods using DPEGT, UC, and the miRCURy kit.

## Reverse Transcription Quantitative Polymerase Chain Reaction (RT-qPCR)

For reverse transcription, the mature sEV-derived miRNAs were reverse transcribed through the miScript II RT kit (Qiagen, Cat#218161). According to the manufacturer's protocol, 3 μL of RNA was mixed with 5X HiSpec buffer, 10X Nucleic mix, and Reverse transcriptase then the reaction was set up for 60 min at 37˚C followed by 5 min at 95˚C. cDNA was later diluted to final concentration of 3 ng/μL for RT- qPCR using miScript SYBR Green PCR Kit (Qiagen, Cat#218073), mixed with 5 μL Qiagen SYBR Green Master Mix, universal primer, and miRNA specific upstream primer in Step One Plus Detection System (Applied Biosystems, CA, USA). The RT-qPCR thermal profile was set to 95˚C for 15 min, 40 cycles of 94˚C for 15 sec, 55˚C for 30 sec, and 70˚C for 30 sec followed by melting curve detection according to the manufacturer's instructions. Relative to healthy controls, fold change of miRNA expression was calculated using the $2^{-\Delta\Delta Ct}$ method and normalized to a combination of reference miRNAs; cel-miR-39 (exogenous control, MS00019789), miR-16-3p (endogenous control, MIMAT0000069), and RNU6B (endogenous ribonuclear RNA, 001093) as no well-established set of internal controls for EV-encapsulated miRNA expression analysis have not yet been identified [22–25]. The

stability of these reference miRNAs was evaluated via RefFinder; a web-based tool that integrates four computational programs (Delta-Ct, GeNorm, Normfinder, and BestKeeper) and assigns a geometric mean value for each reference miRNA based on the overall ranking obtained from each of the four statistical algorithms [26]. Five miRNAs: miR-19a-3p (MS00003192), miR-129-5p (MS00008589), miR-181b-5p (MS00006699), miR-222-3p (MS00007609), and let-7a-5p (MS00031220), were primarily screened in breast cancer patients (n = 6), then we specifically focused on sEV miRNAs that may emerge as candidate biomarkers for IBC. All primers were purchased from Qiagen.

## Bioinformatical analysis for miRNA target genes and pathways prediction

The Kyoto Encyclopedia of Genes and Genome (KEGG) pathways associated with miR-181b-5p, miR-222-3p, and let-7a-5p were analyzed in miRPath DIANA software (version 3.0) [27] based on the TarBase database (version 7.0). For the prediction of miR-181b-5p, miR-222-3p, and let-7a-5p target genes miRbase database (miRDB) (http://mirdb.org/index.html) [28, 29] was used and all the target genes with a score > 95 were selected. Then, the online Database for Annotation, Visualization and Integrated Discovery (DAVID) software was employed to analyzed the gene ontology (GO) Function and KEGG pathways associated to the target genes of miR-181b-5p, miR-222-3p, and let-7a-5p. DAVID software uses well-known classification systems, including GO, KEGG, and BioCarta path (https://david.ncifcrf.gov/home.jsp) [30, 31]. A false discovery rate (FDR) < 0.05 was chosen as the cut-off criterion. Finally, the integration of the protein-protein interaction (PPI) network and the identification of significant candidate genes (Hub Genes) and pathways were performed with the online platform STRING (https://string-db.org), that uses GO, Protein families (Pfam), and KEGG databases to predict PPI networks [32]. First, all the target genes of miR-181b-5p, miR-222-3p, and let-7a-5p were uploaded to String to obtain a single network. Then, the PPI network was exported to Cytoscape software (version 3.8.0) [33] for further network analyses. The Cytoscape plugin Molecular Complex Detection (MCODE) was used to identify the most important clusters or modules from the densely/highly interconnected regions within the network. After set the parameters by the node score cutoff = 0.2, k-core = 2, max. depth from seed = 100, and degree cutoff = 2, we selected four most significative modules with a score > 5, which containing the hub genes. Later, the hub genes were mapped into String to perform an enrichment pathway analysis.

## Statistical analysis

Unless otherwise stated, data are expressed as mean and standard deviation (SD) or standard error mean (SEM). All data were initially tested for normality using Kolomogrov Smirnov and Shapiro-Wilk normality tests. Unpaired Student's t-test was used to compare two normally distributed groups of data, while data of more than 2 groups were analyzed using one-way ANOVA, followed by post hoc tests. The significance between non-parametric variables was evaluated using Chi-square test or Fisher's exact test. The receiver operating characteristic (ROC) curve was calculated based on RQ values. For combined ROC curves, logistic regression models were used to determine the predictive values. The area under the curve (AUC) with 95% CI was calculated for each ROC curve, from which the optimal cut-off point, sensitivity, and specificity of each miRNA were determined. Data were analyzed using both Graph-Pad Prism 8 (GraphPad Software Inc., San Diego, CA, USA) and IBM SPSS advanced statistics version 25 (SPSS Inc., Chicago, IL, USA). Data were considered significant when p-value is < 0.05.

## Results

### Characterization of plasma-derived sEVs

Different transcriptomic and proteomic validation approaches, including DLS, TEM, and western blot were conducted to ascertain the successful isolation of sEVs. First, we isolated sEVs through ultracentrifugation, combined differential centrifugation followed by PEG precipitation (i.e. SPEGT and DPEGT), and the miRCURY Exosome Plasma Kit to evaluate which method could be efficiently employed in the screening of sEV-derived miRNAs as potential biomarkers for IBC relative to non-IBC patients. sEVs heterogeneity was measured in terms of the polydispersity index (PDI), where the lower the PDI, the more monodispersed EV fractions. Based on PDI measurements, EVs with 0.377–0.569 PDI values were isolated using ultracentrifugation and the miRCURY kit, while SPEGT and DPEGT with different concentrations showed 0.558–0.616 and 0.295–0.528 PDI, respectively (Table 1). Notably, the PDI of DPEGT was significantly improved compared to that of SPEGT ($p < 0.05$), indicating that the extra enzymatic and washing steps in DEPGT (8%, PDI = 0.29) have massively enhanced the homogeneity of the retrieved EVs and minimized the polydispersed aggregates. DLS analysis was used to assess the hydrodynamic radius of sEVs and showed that DPEGT and ultracentrifugation resulted in sEVs with an average size less than 200 nm. Of note, the highest intensity was obtained with the 8% DPEGT (Fig 2A). The size distribution of sEVs isolated with different concentrations of SPEGT and DPEGT were compared to ultracentrifugation and miRCURY kit (S1 Fig). In agreement with DLS data, TEM analysis of ultracentrifugation and DPEGT methods showed small rounded or oval-shaped EVs (sEVs) (< 200 nm) with an average size ranging from 75–105 nm for both ultracentrifugation and DEPGT, respectively as depicted in Fig 2B. Western blot analysis of sEVs-enriched pooled fractions by DPEGT (n = 12) confirmed the efficacy of 8% DPEGT in enrichment of sEVs, specifically exosomes. Western blot analysis verified the presence of the Alix, CD63 and HSP70/HSC70 exosomal proteins markers (Fig 2C) using different concentrations of DPEGT compared to miRCURY kit. To further confirm the success of isolation, sEVs were isolated from three different samples namely normal pooled samples (n = 12), non-IBC pooled samples (n = 12) and IBC pooled samples (n = 12) and their western blot analysis unveiled detectable exosomal markers, namely CD63 (tetraspanin) (Fig 2D). On the contrary, no cell organelle contaminating proteins, such as non-exosomal Golgi apparatus protein (GM130) was detected (Fig 2D). We next compared the different approaches employed through the proteomic, transcriptomic yield and purity of enriched plasma sEVs.

### Proteomic content

During the training phase, plasma biopsies were pooled (n = 12) to isolate sEVs using the aforementioned methods and BCA assay was primarily conducted to measure the protein content of sEVs. It was observed that protein content of sEVs increased upon increasing PEG concentration in both single and double treatments, whereby DPEGT generally yielded higher protein content than SPEGT. As depicted in Fig 3, the protein content of sEVs enriched

**Table 1. Polydispersity index (PDI) of plasma sEVs enriched by different procedures.**

| Procedure | UC | miRCURY Kit | SPEGT | | | | | DPEGT | | | | |
|---|---|---|---|---|---|---|---|---|---|---|---|---|
| | | | 5% | 8% | 10% | 12% | 15% | 5% | 8% | 10% | 12% | 15% |
| **PDI** | 0.377 | 0.569 | 0.616 | 0.566 | 0.558 | 0.579 | 0.6 | 0.359 | 0.295 | 0.488 | 0.51 | 0.528 |

UC: ultracentrifugation; SPEGT: single polyethylene glycol treatment; DPEGT: double polyethylene glycol treatment.

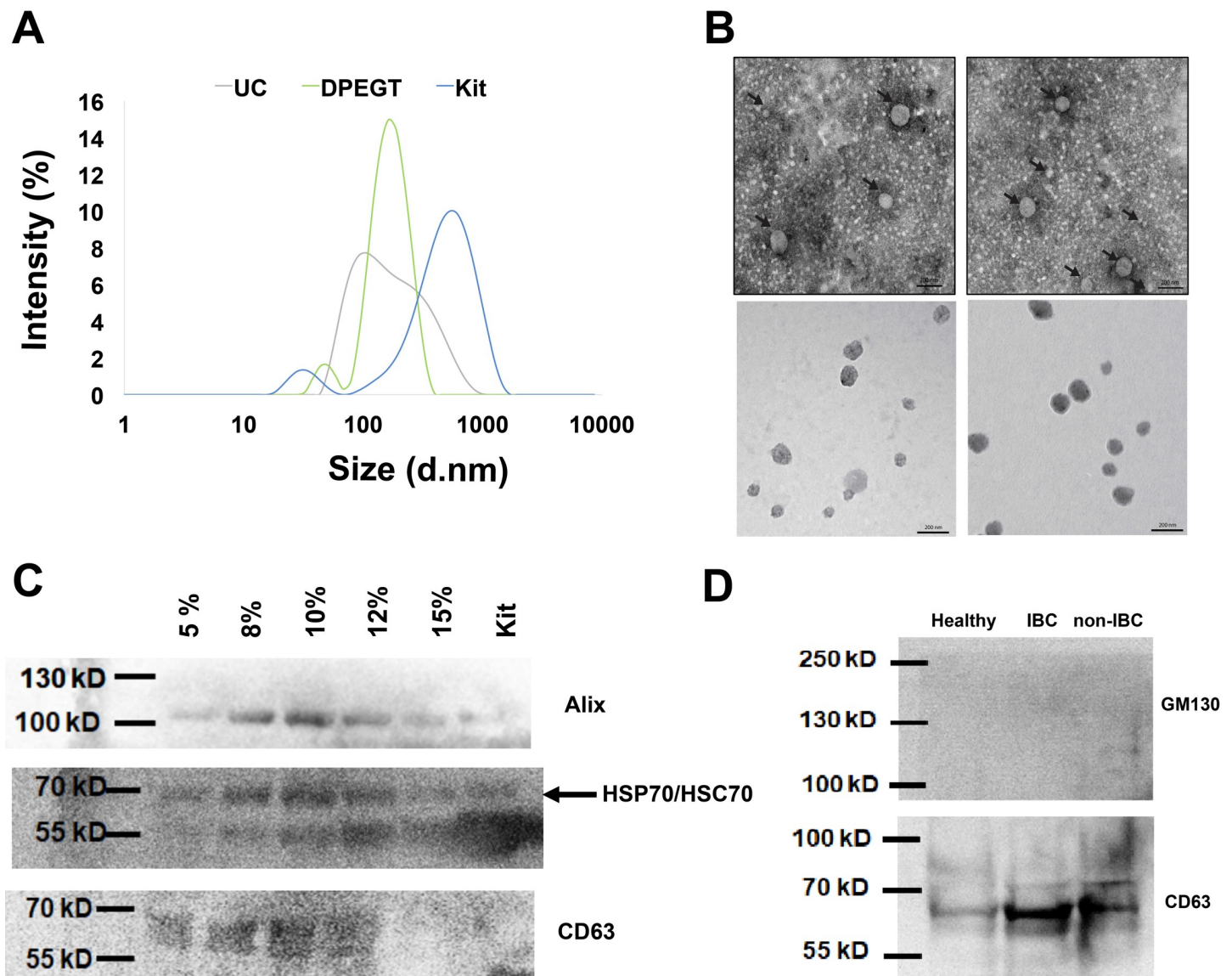https://doi.org/10.1371/journal.pone.0250642.t001

**Fig 2. Characterization of enriched plasma sEVs of breast cancer patients.** The successful isolation of plasma sEVs was verified by different methods. (a) sEVs size distribution was determined by dynamic light scattering (DLS). (b) Transmission electron micrograph of negatively stained sEVs. Size bar equal 200 nm. (c) Western blot of the exosomal proteins markers; Alix, CD63 and HSP70/HSC70 using different concentrations of DPEGT (pooled, n = 12) in comparison to the miRCURY kit. (d) Western blot analysis of the exosomal proteins (e.g., CD63) and non-exosomal Golgi apparatus protein GM130.

through 5% and 15% of DPEGT were significantly higher than those of SPEGT ($p < 0.05$). Also, the protein content of sEVs had a trend of significance with concentrations of 8% ($p = 0.08$), 10% ($p = 0.07$) and 12% ($p = 0.08$) of DPEGT compared with SPEGT (Fig 3). sEVs isolated by the miRCURY kit showed significantly higher protein yield than the 5% and 8% concentrations of SPEGT and DPEGT ($p < 0.001$, for both), whereas ultracentrifugation resulted in limited protein yield compared to 8% ($p < 0.01$), 10% ($p < 0.001$), 12% ($p < 0.001$) and 15% ($p < 0.001$) concentrations of both SPEGT and DPEGT. Collectively, these results suggest that relative to ultracentrifugation, PEG-based methods (SPEGT, DPEGT and the miRCURY kit) may contribute to the enrichment of more plasma sEVs as reflected by higher protein yield.
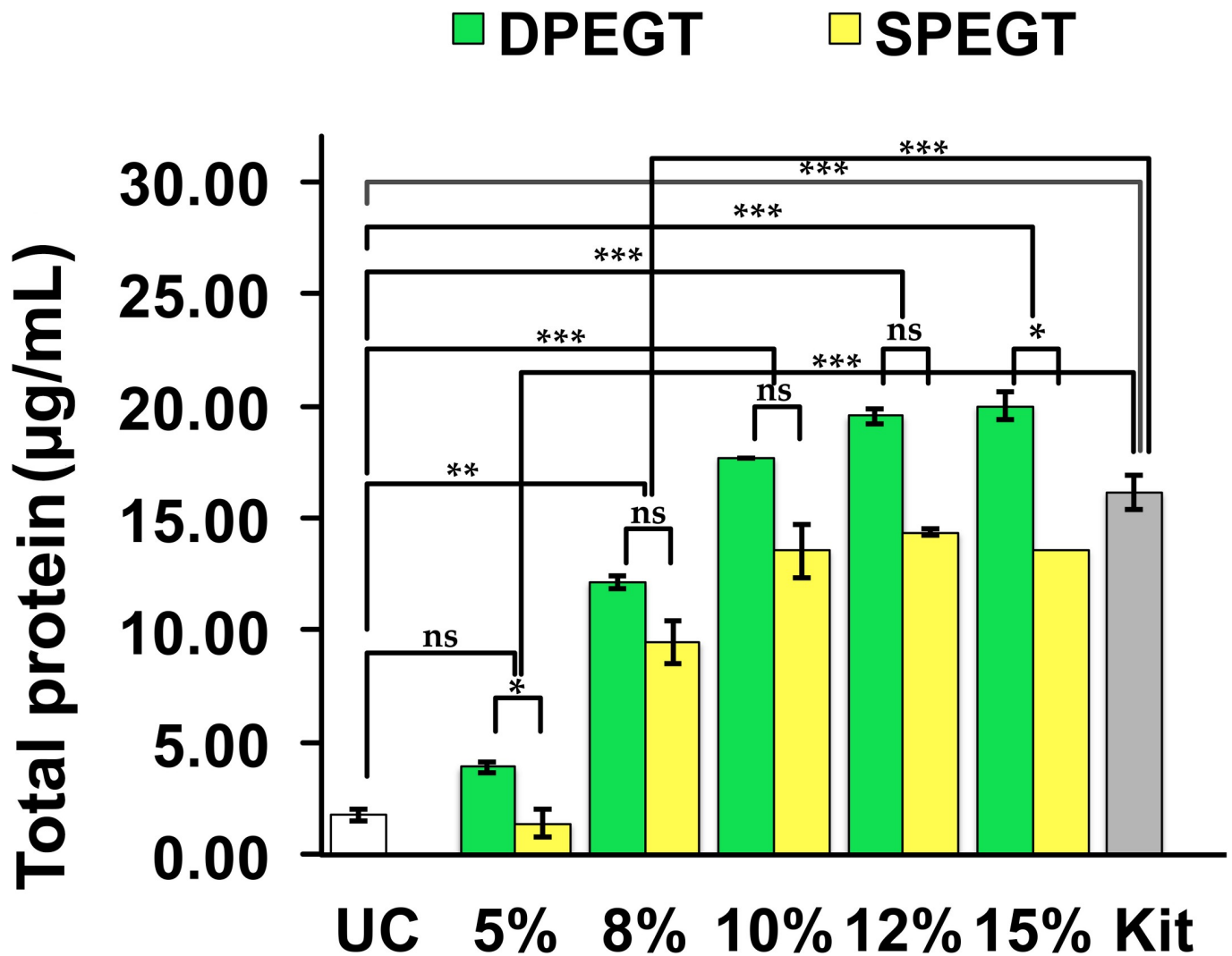
**Fig 3. Total protein content of enriched plasma sEVs.** Isolation of sEVs was conducted by PEG-based methods SPEGT, DPEGT, and the miRCURY kit and UC. Data represent the mean ± SEM, n = 12. *** p < 0.001, ** p < 0.01, * p < 0.05 and ns (not significant) as determined by either Student's t-test or ANOVA test.

### Transcriptomic content

As RNA quantity may reflect the total sEVs yield, total RNA of all isolated sEVs fractions was measured. First, plasma biopsies were pooled for each treatment (n = 12) and total RNA of enriched sEVs with different concentrations of SPEGT and DPEGT was compared to confirm that plasma sEVs were not masked with numerous circulating proteins and total RNA was confined to enriched sEVs, consecutive RNase A and proteinase K treatments of sEVs were used in DPEGT before total RNA extraction. Afterwards, RNA concentration was determined in pooled samples (n = 5) treated with both enzymes and samples (n = 5) treated with only RNase A. Samples treated with Proteinase K had significantly 3.6-fold higher RNA content than those without proteinase K treatment ($p < 0.001$; Fig 4A), which emphasizes that excessive high molecular weight circulating proteins can affect the isolation of sEVs encapsulated RNAs. A significant difference for total RNA yields was observed between different PEG concentrations (p < 0.05), however, total RNA isolated from sEVs by 8% DPEGT was significantly
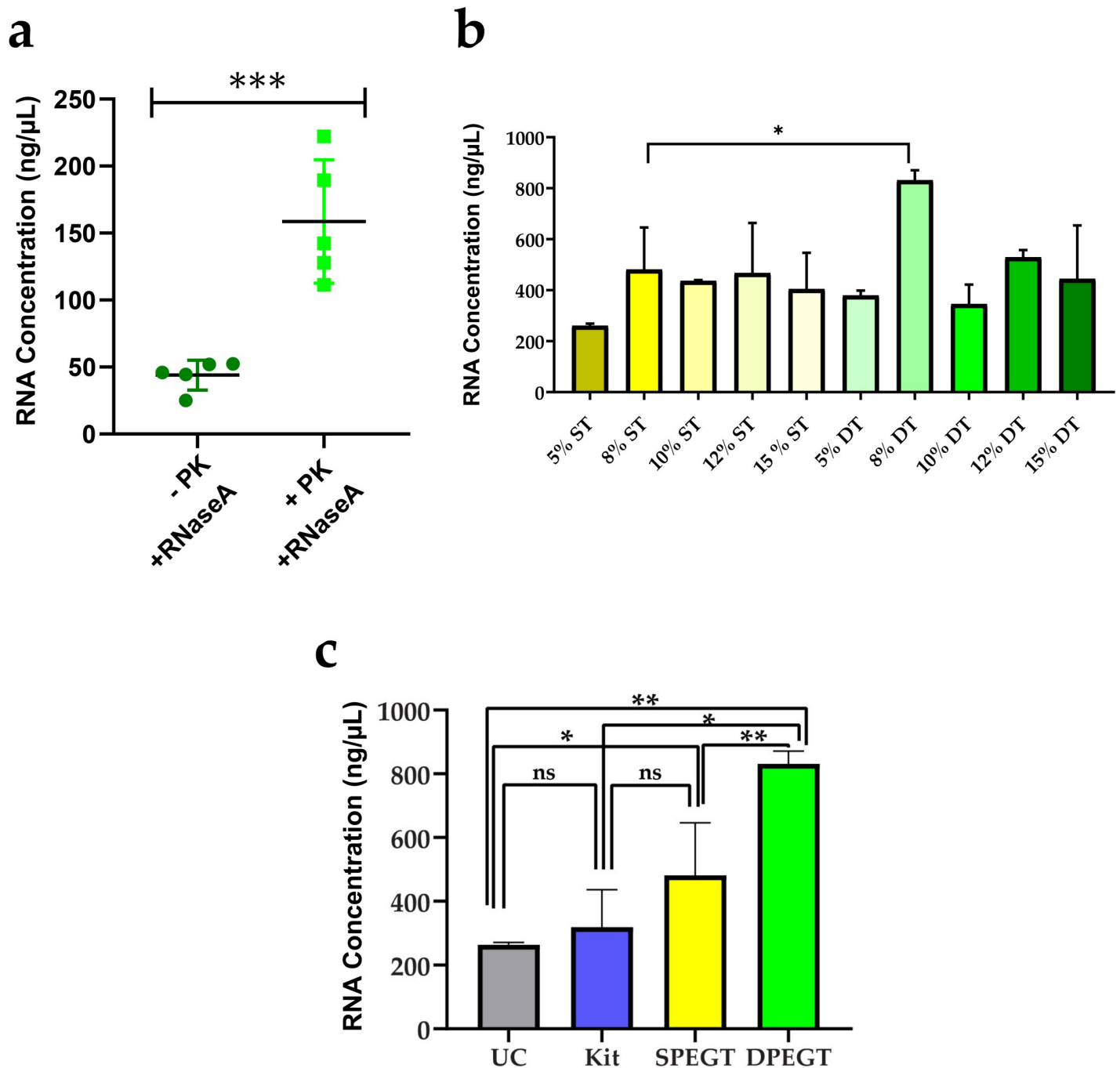
**Fig 4. Total RNA concentration of enriched plasma sEVs.** Isolation of sEVs was conducted by PEG-based methods SPEGT, DPEGT, and miRCURY kit and UC. (a) Effect of RNase A with or without proteinase k (PK) treatment on RNA yield. *** $p < 0.001$ as determined by Student's t-test, n = 5. (b) Effect of single treatment (ST) and double treatment (DT) of PEG with different concentrations on total RNA yield. Data represent the mean ± SEM. * $p < 0.05$ as determined by Student's t-test. (c) Total RNA yield upon 8% SPEGT, 8% DPEGT, miRCURY kit and UC. Data represent the mean ± SEM. ** $p < 0.01$, * $p < 0.05$ and ns (not significant) as determined by either Student's t-test or ANOVA test.

higher than that of SPEGT ($p < 0.05$, Fig 4B). Next, 8% of both SPEGT and DPEGT were compared to the miRCURY kit and ultracentrifugation. DPEGT with 8% significantly increased sEV-derived RNA content compared to other methods ($p < 0.01$; Fig 4C). Moreover, as

depicted in Fig 4C, 8% DPEGT significantly increased sEV-derived RNA yield by relative to ultracentrifugation (by 4-fold; $p < 0.01$), SPEGT ($p < 0.01$) and the miRCURY kit ($p < 0.05$).

## Expression profile of plasma sEV-derived miRNAs in IBC versus non-IBC

We have recently discovered differentially expressed miRNAs in IBC tumors relative to non-IBC as tissue biomarkers, using human breast cancer miRNA PCR array [34]. To extend our findings and to identify sEV-derived miRNAs as non-invasive blood-based biomarkers for IBC, we selected five miRNAs (miR-19a, miR-129-5p, miR-181b-5p, miR-222-3p, and let-7a-5p). We analyzed the expression level of the spike in cel-miR-39 in pooled plasma sEVs (n = 3) enriched by 8% of both SPEGT and DPEGT. A statistically significant difference in the Ct value of cel-miR-39 was detected between DPEGT and SPEGT (p < 0.001, Fig 5A). Notably, no significant difference was detected in the Ct values of cel-miR-39, miR-16-5p, miR-181b-5p, miR-222-3p and let-7a-5p ($p > 0.05$ for all, Fig 5B). Therefore, we used DPEGT to enrich IBC and non-IBC plasma sEVs and quantify their differential miRNA expression pattern. Clinical-pathological features of IBC and non-IBC patients are depicted in Table 2. There was no significant difference in age, lymphovascular invasion, lymph node status, tumor size, tumor grade, or receptor status between IBC and non-IBC patients. However, a significant difference was found in tumor stage between IBC and non-IBC patients ($p < 0.0001$). We quantified the expression levels of miR-19a, miR-129-5p, miR-181b-5p, miR-222-3p, and let-7a-5p in enriched plasma of sEVs of patients with non-IBC (n = 34) and IBC (n = 23) relative to the expression of healthy volunteers (n = 20) by qPCR. To normalize the expression level of sEV-derived miRNAs, three reference/housekeeping controls (cel-miR-39, miR-16-3p, and RNU-6) were selected and their comprehensive stability was evaluated using computational ReFfinder software. According to their geometric mean, reference controls cel-miR-39, miR-16-3p, and RNU-6 were ordered and ranked as 1.19, 1.89, and 2.28 stability values, respectively (S2 Fig). Out of the five sEV-derived miRNAs, three miRNAs showed a significantly differential expression between IBC and non-IBC patients. miR-181b-5p and miR-222-3p expression levels were significantly up-regulated (> 2-fold) (Fig 5C; $p < 0.0001$ and Fig 5D; $p < 0.01$), whereas let-7a-5p was significantly down-regulated (< 0.5-fold) (Fig 5E; $p < 0.0001$) in enriched plasma sEVs of IBC relative to those of non-IBC patients. In contrast, miR-19a and miR-129-5p expression levels were not significantly altered. Next, we compared expression levels of miR-181b-5p, miR-222-3p, and let-7a-5p in enriched plasma sEVs of IBC patients (n = 23) with those of stage-matched non-IBC patients (stage III, n = 10). Interestingly, similar findings were observed with significantly elevated expression levels of miR-181b-5p ($p < 0.001$, Fig 5F) and miR-222-3p ($p < 0.01$, Fig 5G), whilst expression levels of let-7a-5p were significantly downregulated ($p < 0.001$, Fig 5H) in enriched plasma EVs of IBC relative to non-IBC patients. However, when we stratified non-IBC according to tumor stage, no significant difference was observed for the expression levels of the 3-miRNAs between stage III (n = 10) vs. stage I & II (n = 24) ($p > 0.05$, S3 Fig). Finally, we compared the expression levels of the three miRNAs in non-IBC patients treated with neoadjuvant chemotherapy (n = 12) relative to untreated non-IBC (n = 19). Expression levels of only let-7a-5p were significantly diminished in treated non-IBC relative to untreated group ($p < 0.01$, S4 Fig). However, we did not detect any significant alterations in miR-181-5p or miR-222-3p expression levels between treated and untreated patients ($p > 0.05$, S4 Fig).

## Correlations between the expression levels of miR-181b-5p, miR-222-3p and let-7a-5p

Pearson's correlation analysis was used to determine the correlation between miR-181b-5p, miR-222-3p and let-7a-5p in IBC and non-IBC patients. A positive correlation between miR-
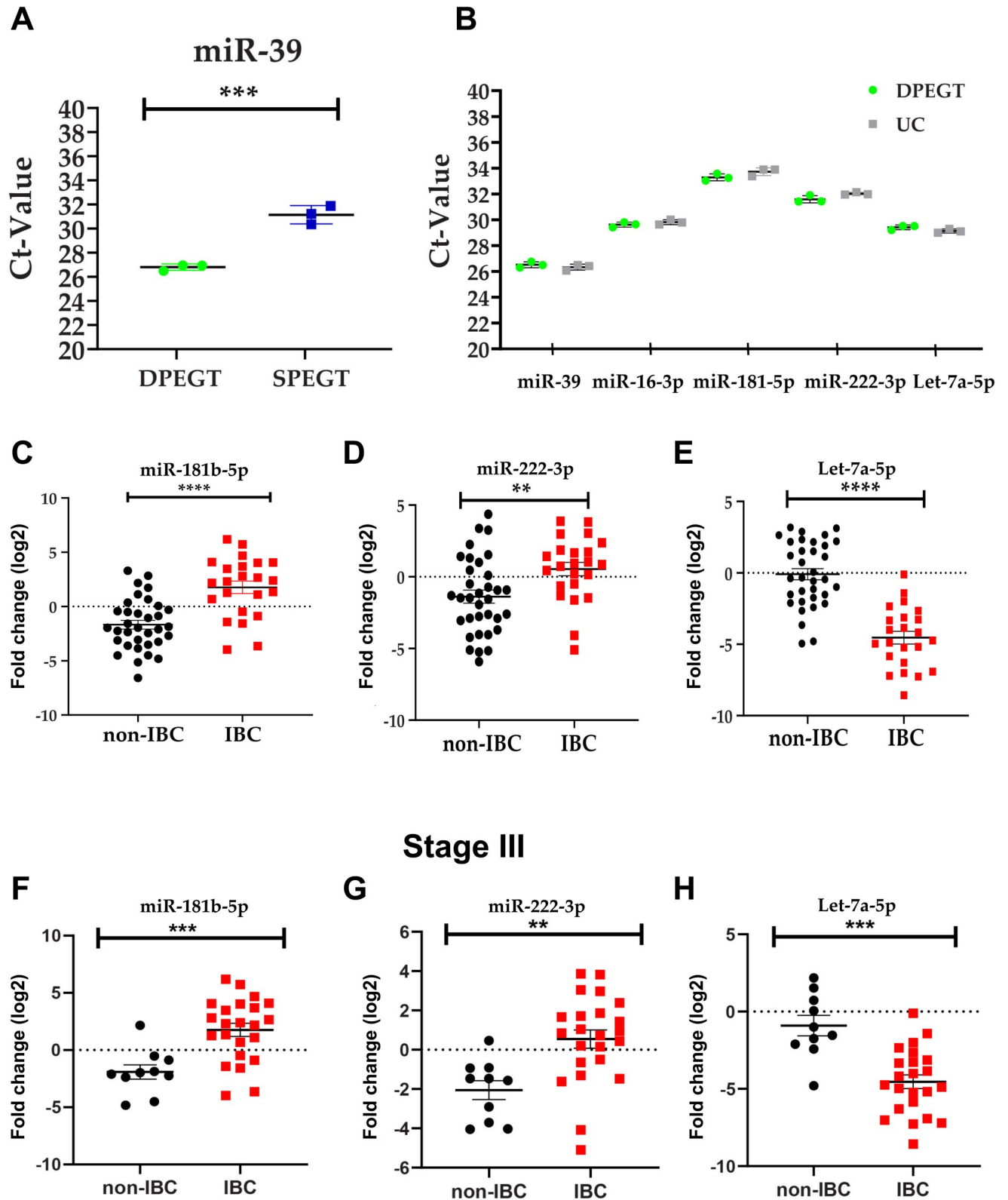
**Fig 5. Expression levels of miR-181b-5p, miR-222-3p and let-7a-5p in enriched plasma sEVs.** Total RNA of sEVs isolated from patients with non-IBC and IBC, and normal volunteers was reverse transcribed into cDNA and miRNA expression levels were quantified using specific miRNAs primers. (a) Ct values of spike in miR-39. n = 3, *** p < 0.001 as determined by Student's t-test. (b) Comparable Ct values of miR-39, miR-16-3p, miR-181b-5p, miR-222-

3p, and let-7a-5p of enriched pooled plasma sEVs isolated by DPEGT and UC, n = 3. Relative expression levels of miR-181b-5p (c), miR-222-3p (d), and let-7a-5p (e) in enriched plasma sEVs isolated from IBC (n = 23) and non-IBC (n = 34) by DPEGT. **** p < 0.0001, ** p < 0.01 as determined by Student's t-test. Relative expression levels of miR-181-5p (f), miR-222-3p (g) and let7-5p (h) in enriched plasma sEV isolated from stage III of both IBC (n = 23) and non-IBC (n = 10) by DPEGT. *** p <0.001, ** p < 0.01 as determined by Student's t-test.

181b-5p and miR-222-3p expression levels was detected in IBC (r = 0.679, $p < 0.001$) and non-IBC (r = 0.675, $p < 0.001$) (Fig 6A). Likewise, a positive correlation was noticed between the expression levels of miR-222-3p and let-7a-5p in IBC (r = 0.459, $p < 0.05$) and non-IBC (r = 0.662, $p < 0.001$) (Fig 6B). Although a significant correlation was observed between miR-181b-5p and let-7a-5p in non-IBC (r = 0.347, $p < 0.05$), no association was detected in IBC patients (r = 0.191, $p > 0.05$) (Fig 6C).

## Diagnostic values of sEV-derived miR-181b-5p, miR-222-3p and let-7a-5p

We next assessed the diagnostic values of let-7a-5p, miR-181b-5p, and miR-222-3p by ROC curve analysis to discriminate IBC from non-IBC patients. ROC curves revealed their potential as candidate non-invasive sEV-encapsulated biomarkers, where let-7a-5p was the best individual diagnostic biomarker with an AUC of 0.9188 and optimal cutoff value of -2.255 (87% sensitivity and 85.3% specificity; $p < 0.001$) (Fig 7A), miR-181b-5p showed an AUC of 0.826

**Table 2. Clinic-pathological features of non-IBC and IBC patients.**

| Group Characteristics | | non-IBC | IBC | p-value |
|---|---|---|---|---|
| | | n = 34 | n = 23 | |
| Age (Years) | Range | 25–70 | 36–71 | 0.23 [a] |
| | Mean (SEM) | 47.41 ± 0.11 | 51.72 ± 0.15 | |
| Tumor Size (cm), n% | ≥4 | 19 (56) | 14 (61) | 0.60 [b] |
| | < 4 | 15 (44) | 9 (39) | |
| Tumor Grade, n% | I | 3 (9) | 2 (9) | 0.75 [b] |
| | II | 24 (71) | 17 (74) | |
| | III | 7 (21) | 4 (17) | |
| Tumor Stage | I and II | 24 (71) | 0 | < 0.0001[b] |
| | III | 10 (29) | 23 (100) | |
| Lymphovascular Invasion, n% | Positive | 13 (38) | 12 (52) | 0.20 [b] |
| | Negative | 21 (62) | 11 (48) | |
| Lymph Nodes, n% | ≥4 | 15 (44) | 12 (52) | 0.21 [b] |
| | < 4 | 19 (56) | 11 (48) | |
| ER, n% | Positive | 23 (68) | 13 (57) | 0.41 [b] |
| | Negative | 11 (32) | 9 (39) | |
| | NA | 0 | 1 (4) | |
| PR, n% | Positive | 24 (71) | 12 (52) | 0.18 [b] |
| | Negative | 10 (29) | 10 (43) | |
| | NA | 0 | 1 (4) | |
| Her-2, n% | Positive | 10 (29) | 10 (43) | 0.15 [b] |
| | Negative | 24 (71) | 12 (52) | |
| | NA | 0 | 1 (4) | |

Data are expressed as mean ± SEM, NA Data not available

* Significant p value calculated by [a]Student's t-test or [b]Pearson Chi-Square. ER, estrogen receptor; PR, progesterone receptor; Her-2, human epidermal growth factor receptor-2.
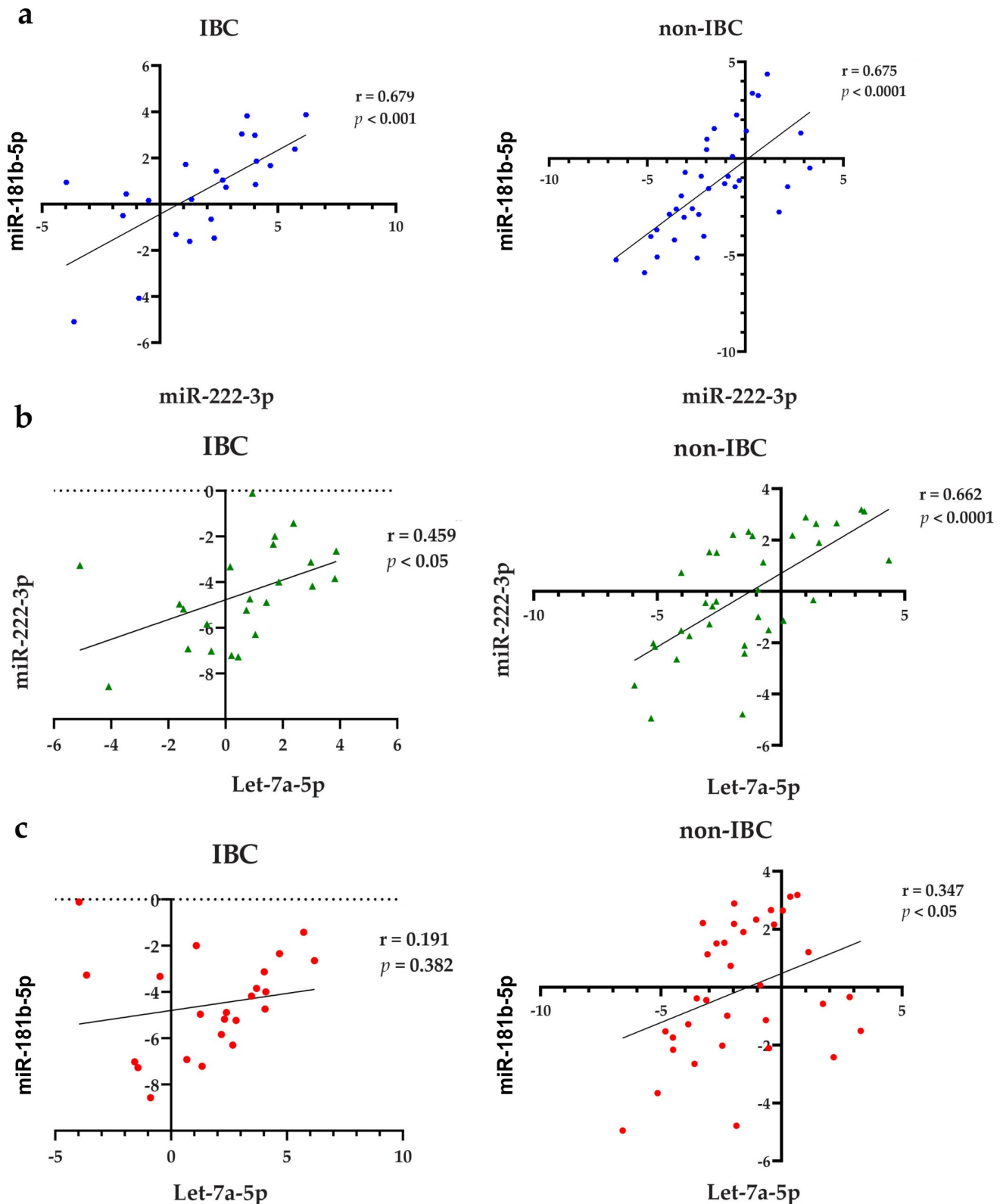
**Fig 6. Pearson's correlation analysis between miR-181b-5p, miR-222-3p, and let-7a-5p expression in sEVs.** (a) A significant positive correlation between miR-181b-5p and miR-222-3p in IBC (left panel) and non-IBC (right panel). (b) A significant positive correlation between miR-222-3p and let-7a-5p in IBC (left panel) and non-IBC (right panel). (c) A significant positive correlation between miR-181b-5p and let-7a-5p in non-IBC (right panel), but not in IBC (left panel).
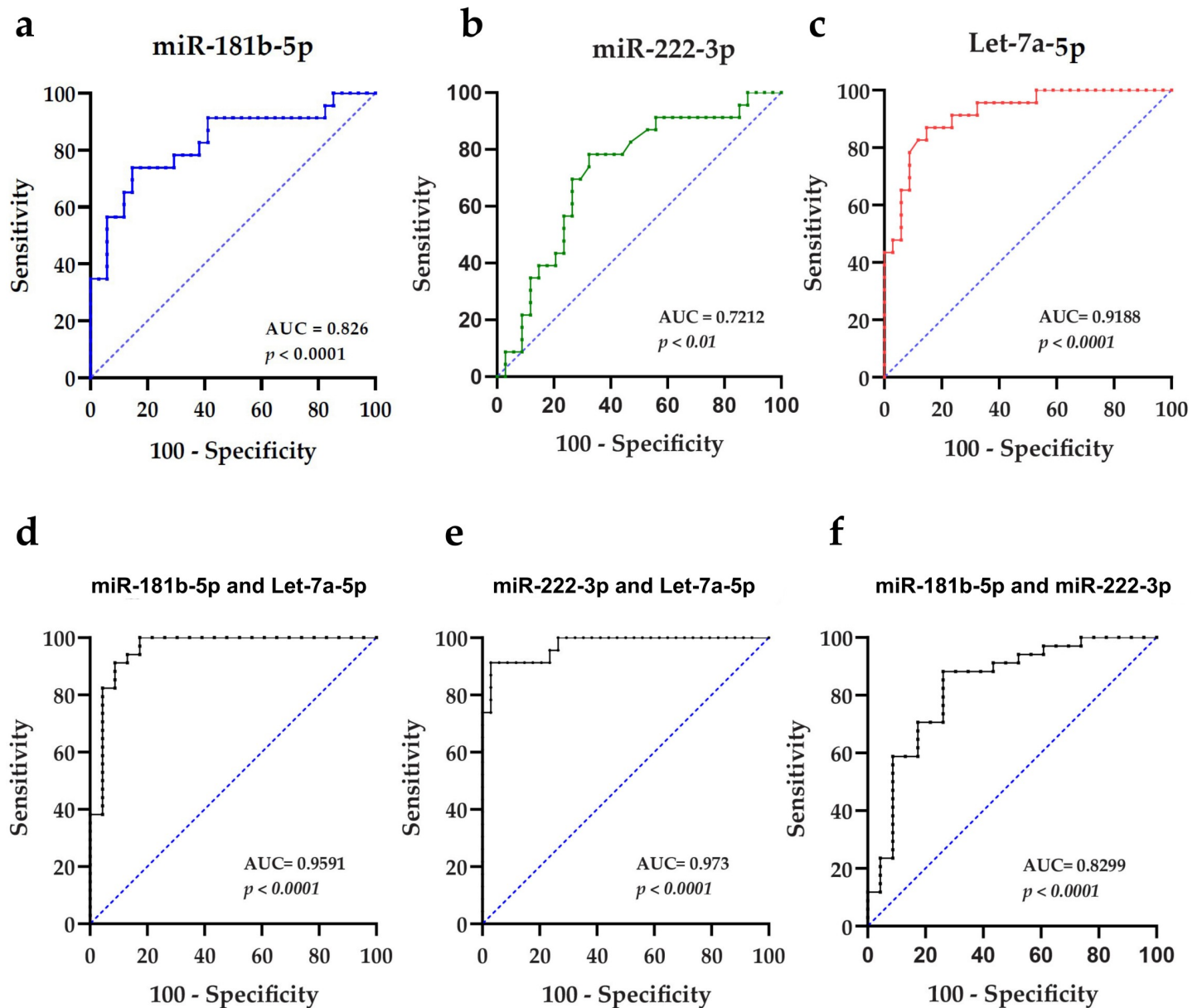
**Fig 7. ROC curves generated using expression levels of miR-181b-5p, miR-222-3p, and let-7a-5p.** (a-c) ROC curves generated using individual miRNA, namely miR-181b-5p, miR-222-3p, and let-7a-5p, respectively. (d-f) ROC curves generated using a combination of expression levels of miR-181b-5p and let-7a-5p, miR-222-3p and let-7a-5p, and miR-181b-5p and miR-222-3p as a miRNA panel to discriminate non-IBC and IBC patients, respectively.

(73.9% sensitivity and 85.3% specificity; $p < 0.001$) (Fig 7B), and miR-222-3p had an AUC of 0.7212 (78.3% sensitivity and a 67.6% specificity; $p < 0.01$) (Fig 7C). Further improvement in the discriminatory accuracy of these miRNAs was expected by combination. Thus, we applied different binary logistic regression models with non-IBC as a reference category; each couple of miRNAs was combined and the positive predictive value (PPV), negative predictive value (NPV), sensitivity, specificity, and optimal cutoff values for each model were evaluated (Table 3). Using the logistic regression model, we assessed the predictive potential of different

**Table 3. ROC curve analysis of individual and combination of sEV-derived miRNAs to differentiate IBC from non-IBC patients.**

| EV- derived miRNAs | let-7a-5p | miR-181b-5p | miR-222-3p | miR-222-3p and let-7a-5p panel | let-7a-5p and miR-181b-5p panel | miR-181b-5p and miRNA-222-3p panel |
|---|---|---|---|---|---|---|
| AUC | 0.919 | 0.826 | 0.721 | 0.973 | 0.959 | 0.830 |
| S. E. | 0.036 | 0.059 | 0.069 | 0.018 | 0.029 | 0.058 |
| 95% CI | 0.85–0.99 | 0.71–0.94 | 0.59–0.86 | 0.93–1.00 | 0.90–1.00 | 0.72–0.94 |
| Optimal Cutoff | -2.255 | 0.670 | -0.685 | 0.533 | 0.742 | 0.494 |
| SN (%) | 87.0% | 73.9% | 78.3% | 91.3% | 82.6% | 73.9% |
| SP (%) | 85.3% | 85.3% | 67.6% | 97.1% | 100% | 88.2% |
| PPV (%) | 85.7% | 76.2% | 60.0% | 95.5% | 87.0% | 81.0% |
| NPV (%) | 86.1% | 80.6% | 70.3% | 94.3% | 91.2% | 83.3% |
| $p$-value | < 0.001 | < 0.001 | < 0.01 | < 0.001 | < 0.001 | < 0.001 |

AUC: area under the curve; CI: confidence interval; SN: sensitivity; SP: specificity; PPV: positive predictive value; and NPV: negative predictive value.

combinations of let-7a-5p, miR-181b-5p, and miR-222-3p expression levels for IBC (Table 4). The best regression model with highest accuracy was the combination of miR-222-3p and let-7a-5p expression, it was statistically significant, $\chi2(2) = 55.19$ (p < 0.001), as it correctly classified 94.0% of cases and explained 83.0% (Nagelkerke R2) of the variance in IBC. As depicted in Table 4, the regression coefficient for let-7a-5p significantly [B = -1.21, OR = 0.30 ($p$ < .001)] showed that upregulated let-7a-5p expression levels were only 0.3 times associated with the likelihood of exhibiting IBC ($p$ < 0.01); in other words, downregulated let-7a-5p was significantly associated with the likelihood of exhibiting IBC. While the regression coefficient for miR-222-3p significantly [B = 0.81, OR = 2.25 (p = 0.003)] indicated that the upregulated miR-222-3p expression levels were 2.25 times more in IBC than non-IBC (p < 0.05). Hence, the ROC curve analysis of miR-222-3p and let-7a-5p panel significantly improved the AUC to 0.973 with the highest sensitivity (91.3%) and specificity (97.1%) values (p < 0.001) (Fig 7D). Of note, let-7a-5p and miR-181b-5p panel also presented an improved an AUC of 0.959 with 82.6% sensitivity and 100% specificity (p < 0.001) (Fig 7E). A combination of miR-181b-5p and miR-222-3p showed a 0.83 AUC value with a sensitivity of 73.9% and 88.2% specificity (Fig 7F). Taken together, these results suggest that sEV-derived let-7a-5p, a panel of sEV-encapsulated let-7a-5p and miR-181b-5p or let-7a-5p and miR-222-3p are promising biomarkers for accurate diagnosis of IBC.

## Prediction of miR-181b-5p, miR-222-3p and let-7a-5p target genes, GO function and KEGG pathway analysis

To identify the potential target genes of miR-181b-5p, miR-222-3p, and let-7a-5p we used the miRbase database (miRDB). After selecting all target genes of score > 95, we found 204 target

**Table 4. Logistic regression miRNAs combination models for IBC diagnosis.**

| EV-derived miRNAs | | B | SE | 95% CI | OR | Percentage Accuracy in classification (PAC) | Nagelkerke R² (%) | p-value |
|---|---|---|---|---|---|---|---|---|
| miR-222-3p and let-7a-5p panel | miR-222-3p | 0.811 | 0.27 | [0.28, 1.34] | 2.25 | 94.7% | 83.8% | < 0.01 |
| | let-7a-5p | -1.211 | 0.35 | [-1.89, -0.53] | 0.30 | | | < 0.001 |
| Let-7a-5p and miR-181b-5p panel | let-7a-5p | -0.915 | 0.29 | [-1.48, -0.35] | 0.40 | 89.5% | 78.1% | < 0.001 |
| | miR-181b-5p | 0.442 | 0.15 | [0.15, 0.74] | 1.56 | | | < 0.001 |
| miR-181b-5p and miRNA-222-3p panel | miR-181b-5p | 0.543 | 0.17 | [0.21, 0.88] | 1.72 | 82.5 | 41.2% | < 0.001 |
| | miRNA-222-3p | -0.061 | 0.17 | [-0.40, 0.28] | 0.94 | | | 0.724 |

B: Beta regression coefficient; SE: Standard Error; 95% CI: confidence interval; OR: Odds Ratio.

**Table 5. GO analysis of miR-181b-5p, miR-222-3p and let-7a-5p target genes.**

| Category | Term | Count | % | p-value |
|---|---|---|---|---|
| **Biological process** | Regulation of transcription, DNA-templated | 37 | 18.9 | 2.60E-06 |
| | Transcription, DNA-templated | 41 | 20.9 | 2.90E-05 |
| | Anterior/posterior pattern specification | 6 | 3.1 | 1.60E-03 |
| | Positive regulation of transcription from RNA polymerase II promoter | 22 | 11.2 | 1.70E-03 |
| | Negative regulation of transcription from RNA polymerase II promoter | 18 | 9.2 | 1.70E-03 |
| | Somatic stem cell population maintenance | 5 | 2.6 | 5.00E-03 |
| | 3'-UTR-mediated mRNA destabilization | 3 | 1.5 | 6.90E-03 |
| | Insulin-like growth factor receptor signaling pathway | 3 | 1.5 | 9.40E-03 |
| **Cellular component** | Nucleus | 83 | 42.3 | 4.30E-05 |
| | Intracellular | 27 | 13.8 | 1.30E-03 |
| | Endosome | 9 | 4.6 | 2.40E-03 |
| | Heterochromatin | 3 | 1.5 | 2.00E-02 |
| | Histone methyltransferase complex | 3 | 1.5 | 2.30E-02 |
| | Glycerol-3-phosphate dehydrogenase complex | 2 | 1 | 3.10E-02 |
| | Cytoplasmic vesicle membrane | 5 | 2.6 | 4.20E-02 |
| | Heterotrimeric G-protein complex | 3 | 1.5 | 4.60E-02 |
| **Molecular function** | DNA binding | 39 | 19.9 | 4.10E-06 |
| | Metal ion binding | 43 | 21.9 | 1.90E-05 |
| | Transcription factor activity, sequence-specific DNA binding | 23 | 11.7 | 5.10E-04 |
| | SMAD binding | 5 | 2.6 | 1.10E-03 |
| | Nucleic acid binding | 22 | 11.2 | 1.70E-03 |
| | Methylated histone binding | 4 | 2 | 1.80E-02 |
| | Transcriptional repressor activity, RNA polymerase II core promoter proximal region sequence-specific binding | 5 | 2.6 | 3.00E-02 |
| | Zinc ion binding | 20 | 10.2 | 4.00E-02 |

genes for the three miRNAs. Then, to analyze the functional and network pathways of the selected 204 miRNAs targets, we employed the DAVID tool. The GO analysis showed the biological process (BP), cellular component (CC), and the molecular function (MF) related to all the miRNAs target genes. Table 5 shows the most eight significant terms ($p < 0.05$) in each category. In the BP category, the regulation of transcription, somatic stem cell population maintenance, mRNA destabilization and insulin growth factor receptor signaling pathway were mainly enriched. The CC category was enriched in the terms of nucleus, intracellular, endosome, heterochromatin, cytoplasmic vesicle membrane, and histone methyl transferase, glycerol-phosphate dehydrogenase, and heterotrimeric G-protein complex. Finally, DNA, metal ion, SMAD, nucleic acid, methylated histone, and transcriptional repressor activity, RNA polymerase II core promoter proximal region sequence-specific binding were enriched in the MF. Finally, the KEGG analysis demonstrated that different pathways that have been associated to cancer, including signaling pathways related to stem cells, FoxO, GABAergic and cholinergic synapse, PI3K-AKT, and Rap1 were mainly enriched (Table 6).

## Identification of hub genes and enrichment pathways from miR-181b-5p, miR-222-3p and let-7a-5p targets PPI networks

In order to identify the hub genes, we first obtained the PPI regulatory network of the all 204 miRNAs targets. For this purpose, we used String database selected a medium score > 0.4 to construct the network. We observed a huge network in which almost all the genes were interconnected (S5 Fig). After that, the network was imported to the Cytoscape tool to obtain the

**Table 6. Kyoto Encyclopedia of Genes and Genomes (KEGG) enrichment pathway analysis of miR-181b-5p, miR-222-3p and let-7a-5p target genes.**

| Term | Count | % | *p*-value |
|---|---|---|---|
| Signaling pathways regulating pluripotency of stem cells | 7 | 3.6 | 1.10E-03 |
| FoxO signaling pathway | 6 | 3.1 | 5.20E-03 |
| GABAergic synapse | 5 | 2.6 | 5.50E-03 |
| PI3K-Akt signaling pathway | 9 | 4.6 | 7.90E-03 |
| Rap1 signaling pathway | 7 | 3.6 | 8.10E-03 |
| MicroRNAs in cancer | 8 | 4.1 | 9.70E-03 |
| Melanogenesis | 5 | 2.6 | 9.80E-03 |
| Cholinergic Synapse | 5 | 2.6 | 1.40E-02 |
| Pathways in cancer | 9 | 4.6 | 1.60E-02 |
| Morphine addiction | 4 | 2 | 4.10E-02 |

https://doi.org/10.1371/journal.pone.0250642.t006

hub genes. The MCODE plug in Cytoscape was used to find the modules in which the hub genes were present. S1 Table shows the 10 clusters or modules obtained after the analysis. The top four significative modules with a score > 5 in which the hub genes are present were selected. Of a total of 204 genes analyzed, 38 are hub genes. In the first module there are 19 genes, in the second module 9 and in the third and fourth module 5 genes each (S1 Table). It is very important to explore the pathways that are potentially regulated by these hub genes. To this end, the genes of each module were uploaded to the String database to obtain the PPI network and the enriched KEGG pathways of each module. At first, it was noted that all the genes of each module were highly interconnected (Fig 8A–8D). The top 10 significant ($p < 0.05$) enrichments for module 1 and 2, while only five enrichments for module 3, and two enrichments for module 4 were selected to be represented in the tables in Fig 8A–8D. The hub genes in module 1 were associated with the regulation of chemokine, apelin, and relaxin signaling pathways, cholinergic, GABAergic, glutamatergic, and serotonergic synapse, circadian, morphine addiction, and alcoholism (Fig 8A). Interestingly, the hub genes in module 2 potentially regulate pathways associated to cancer such as p53 and PI3K-AKT signaling, cell cycle, cellular senescence, small cell lung and prostate cancer, and viral carcinogenesis (Fig 8B). On the other hand, the hub genes of module 3 have an impact on vesicular transport, synaptic vesicle circle, insulin secretion, autophagy, and platelet activation (Fig 8C). Finally, hub genes in module 4 were more associated with cell cycle and meiosis (Fig 8D).

## Pathways associated with miR-181b-5p, miR-222-3p and let-7a-5p expression

We used the DIANA miRPath online tool to obtain the KEGG enrichment pathways of miR-181b-5p, miR-222-3p, and let-7a-5p. We found 26 pathways with significant *p*-values, there were common pathways that all three miRNAs share including p53 signaling and ubiquitin mediated proteolysis (Table 7 and S6 Fig). On the other hand, let-7a-5p was associated with pathways related to cancer, such as TGF-β, thyroid hormone signaling, transcriptional misregulation, other pathways in cancer, colorectal carcinoma, chronic myeloid leukemia, Hepatitis B, endocytosis and viral carcinogenesis (Table 7 and S6 Fig). miR-222-3p and let-7a-5p shared the enrichment of HTLV-infection, arrhythmogenic cardiomyopathy, lysine degradation, and cell cycle signaling. The enrichment of Hippo signaling and proteoglycans in cancer were associated with miR-181b-5p and let-7a-5p. miR-181b-5p has an important regulatory role in prostate and renal cell cancer, whilst miR-222-3p regulates cell adhesion molecules (Table 7 and S6 Fig).

**a**
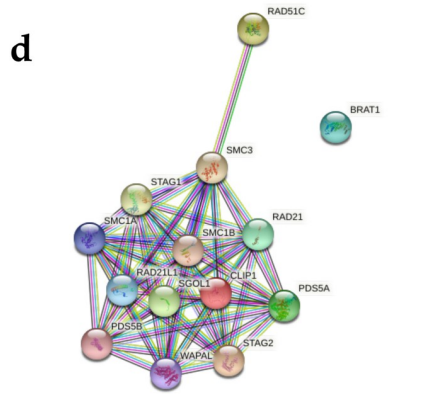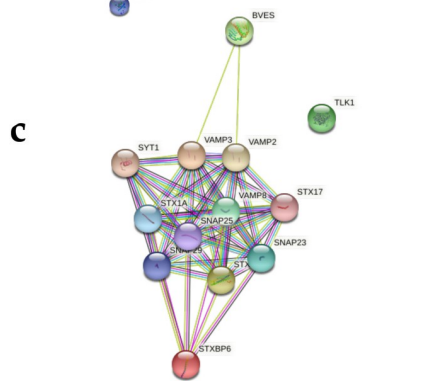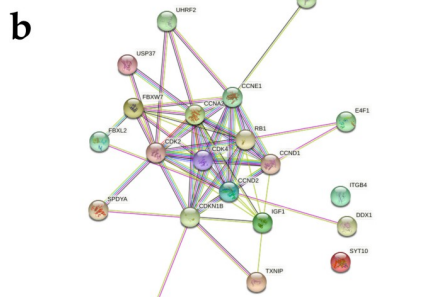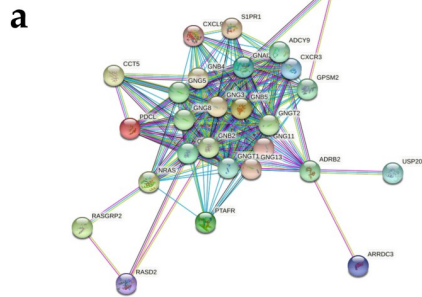
| Term ID | Term | Observed genes | False discovery rate | Genes |
|---|---|---|---|---|
| hsa04062 | Chemokine signaling pathway | 17 | 5.23E-26 | GNB3, GNB4, GNG13, GNG11, GNGT1, GNB5, ADCY9, GNG3, GNG8, GNB2, RASGRP2, CXCL9, NRAS, GNAI3, GNG5, CXCR3, GNGT2 |
| hsa04725 | Cholinergic synapse | 14 | 9.32E-23 | GNB3, GNB4, GNG13, GNG11, GNGT1, GNB5, ADCY9, GNG3, GNG8, GNB2, NRAS, GNAI3, GNG5, GNGT2 |
| hsa04371 | Apelin signaling pathway | 14 | 4.93E-22 | GNB3, GNB4, GNG13, GNG11, GNGT1, GNB5, ADCY9, GNG3, GNG8, GNB2, NRAS, GNAI3, GNG5, GNGT2 |
| hsa04713 | Circadian entrainment | 13 | 4.93E-22 | GNB3, GNB4, GNG13, GNG11, GNGT1, GNB5, ADCY9, GNG3, GNG8, GNB2, GNAI3, GNG5, GNGT2 |
| hsa04727 | GABAergic synapse | 13 | 4.93E-22 | GNB3, GNB4, GNG13, GNG11, GNGT1, GNB5, ADCY9, GNG3, GNG8, GNB2, GNAI3, GNG5, GNGT2 |
| hsa04926 | Relaxin signaling pathway | 14 | 4.93E-22 | GNB3, GNB4, GNG13, GNG11, GNGT1, GNB5, ADCY9, GNG3, GNG8, GNB2, NRAS, GNAI3, GNG5, GNGT2 |
| hsa05032 | Morphine addiction | 13 | 4.93E-22 | GNB3, GNB4, GNG13, GNG11, GNGT1, GNB5, ADCY9, GNG3, GNG8, GNB2, GNAI3, GNG5, GNGT2 |
| hsa04724 | Glutamatergic synapse | 13 | 4.05E-21 | GNB3, GNB4, GNG13, GNG11, GNGT1, GNB5, ADCY9, GNG3, GNG8, GNB2, GNAI3, GNG5, GNGT2 |
| hsa04726 | Serotonergic synapse | 13 | 4.05E-21 | GNB3, GNB4, GNG13, GNG11, GNGT1, GNB5, GNG3, GNG8, GNB2, NRAS, GNAI3, GNG5, GNGT2 |
| hsa05034 | Alcoholism | 13 | 5.92E-20 | GNB3, GNB4, GNG13, GNG11, GNGT1, GNB5, GNG3, GNG8, GNB2, NRAS, GNAI3, GNG5, GNGT2 |

**b**

| Term ID | Term | Observed genes | False discovery rate | Genes |
|---|---|---|---|---|
| hsa04110 | Cell cycle | 8 | 6.86E-11 | CCND1, CDKN1B, CDK4, CCND2, CCNE1, CDK2, RB1, CCNA2 |
| hsa05203 | Viral carcinogenesis | 8 | 7.23E-10 | CCND1, CDKN1B, CDK4, CCND2, CCNE1, CDK2, RB1, CCNA2 |
| hsa05165 | Human papillomavirus infection | 9 | 8.66E-10 | ITGB4, CCND1, CDKN1B, CDK4, CCND2, CCNE1, CDK2, RB1, CCNA2 |
| Hsa04115 | p53 signaling pathway | 6 | 3.03E-09 | CCND1, CDK4, CCND2, CCNE1, CDK2, IGF1 |
| hsa05161 | Hepatitis B | 7 | 3.03E-09 | CCND1, CDKN1B, CDK4, CCNE1, CDK2, RB1, CCNA2 |
| hsa04218 | Cellular senescence | 7 | 4.47E-09 | CCND1, CDK4, CCND2, CCNE1, CDK2, RB1, CCNA2 |
| hsa05222 | Small cell lung cancer | 6 | 9.66E-09 | CCND1, CDKN1B, CDK4, CCNE1, CDK2, RB1 |
| hsa05215 | Prostate cancer | 6 | 1.14E-08 | CCND1, CDKN1B, CCNE1, CDK2, RB1, IGF1 |
| hsa04151 | PI3K-Akt signaling pathway | 8 | 2.25E-08 | ITGB4, CCND1, CDKN1B, CDK4, CCND2, CCNE1, CDK2, IGF1 |
| hsa05162 | Measles | 6 | 5.61E-08 | CCND1, CDKN1B, CDK4, CCND2, CCNE1, CDK2 |

**c**

| Term ID | Term | Observed genes | False discovery rate | Genes |
|---|---|---|---|---|
| hsa04130 | SNARE interactions in vesicular transport | 8 | 2.28E-18 | VAMP3,SNAP29,STX1A,SNAP23,STX17,VAMP8,VAMP2,STX3 |
| hsa04721 | Synaptic vesicle cycle | 5 | 2.35E-09 | STX1A,SNAP25,SYT1,VAMP2,STX3 |
| hsa04911 | Insulin secretion | 3 | 7.82E-05 | STX1A,SNAP25,VAMP2 |
| hsa04140 | Autophagy - animal | 3 | 0.00019 | SNAP29,STX17,VAMP8 |
| hsa04611 | Platelet activation | 2 | 0.006 | SNAP23,VAMP8 |

**d**

| Term ID | Term | Observed genes | False discovery rate | Genes |
|---|---|---|---|---|
| hsa04110 | Cell cycle | 6 | 1.05E-09 | STAG2, RAD21, SMC1A, SMC1B, SMC3, STAG1 |
| hsa04114 | Oocyte meiosis | 4 | 3.20E-06 | SGOL1, SMC1A, SMC1B, SMC3 |

**Fig 8. Hub genes protein-protein interactions (PPI) and enrichment pathways.** To analyze the hub genes, present in most significant modules obtained from the Cytoscape plugin Molecular Complex Detection (MCODE) we used the String database. (a-d) shows the PPI network of the hub genes present in each module and the enrichment pathways associated to them. < 1.0E-16 is the *p*-value for the entire PPI network of each module. String performs the false discovery rate (FDR) for the statistics.

https://doi.org/10.1371/journal.pone.0250642.g008

## Discussion

In this study we assessed the feasibility of using minimally invasive sEV- encapsulated miRNAs to discriminate IBC from non-IBC patients, as an alternative to invasive tissue biopsies. Our study showed that plasma sEV-encapsulated miR-181b-5p, miR-222-3p and let-7a-5p are potential biomarkers for IBC. Although, in last years, sEV-derived miRNAs showed significant relevance in various clinical and translational applications, the sEVs enrichment procedure could dramatically interfere with downstream applications [35, 36]. A major objective of our study was to optimize a procedure suitable for rapid and economical diagnosis and analysis of sEV-derived miRNAs. Thus, we first optimized the sEVs isolation protocol and compared different concentrations of PEG-based procedures to the gold standard ultracentrifugation and miRCURY exosome kit. We found that precipitating reagents did not only yield more sEVs (< 200nm) as examined by DLS, TEM, protein and RNA analyses, but also resulted in improved reproducibility. However, the miRCURY exosome kit unexpectedly showed broad size distribution in DLS with weak or no sEVs protein markers. This supports that commercial PEG-based kit may co-isolate larger EVs or huge amounts of sEV masking protein aggregates [14, 17]. DPEGT was optimized to specifically isolate sEVs through the combination of proteinase K and RNase A treatments to differentially centrifuged and ultra-filtrated plasma pooled samples. Based on DLS, RNA and protein patterns of isolated sEVs, the overall efficiency of DPEGT in retrieving sEVs was better than that of SPEGT and the miRCURY kit. This is in agreement with Yeing *et al.* [16], who stated that two step PEG-based precipitation was superior to single PEG, although they used different molecular weight of PEG to isolate sEVs from cell line conditioned media and without profiling of sEV-encapsulated miRNAs. Differences between 5, 8, 10, 12 and 15% of DPEGT were only evident through DLS not EV protein markers. Of note, sEV total RNA retrieved and miRNAs quantitative expression levels were significantly improved upon digesting enzymes treatment. Consistently, Moon *et al.* [37], have also highlighted the positive impact of proteinase k on improving different commercial kits purity for plasma EVs isolation. The monodispersed and paramount sEV yields obtained via DPEGT (8% + enzymatic treatment) made it the procedure of choice for subsequent miRNA profiling. Prior to downstream sEV-derived miRNAs analysis, the miRNA differential expression levels were measured, and no significant difference was detected between DPEGT and UC. Our study shows that high yields of sEVs could be efficiently enriched for miRNA profiling through an inexpensive PEG-based method. This is in consistent with Lv *et al.* [18], who used a PEG-based procedure for isolation of miRNAs from urinary exosomes. To test the feasibility of sEV-packaged miRNAs as a promising alternative for invasive tissue biopsies of IBC, we focused on three selected sEV-encapsulated miRNAs (miR-181b-5p, miR-222-3p and let-7a-5p), whose expression levels were detected in IBC tissues, as we recently reported [34].

The selected miRNAs are known for various oncogenic roles in breast cancer regulation as supported by the interaction networks analysis. Hub genes identified were mainly involved in regulation of chemokine signaling pathways, that trigger metastasis of IBC [38]. Based on KEGG pathways analysis, PI3K/AKT pathway that is remarkably activated in IBC [38], was shown to be regulated by these miRNAs. It has been shown that in gastrointestinal tumors miR-222 induces apoptosis through the activation of KIT and AKT pathway [39]. In ovarian

**Table 7. Kyoto Encyclopedia of Genes and Genomes (KEGG) pathways associated with miR-181b-5p, miR-222-3p, and let-7a-5p.**

| KEGG pathway | Associated miRNAs | Number of genes | *p*-value |
|---|---|---|---|
| Lysine degradation | hsa-miR-222-3p | 17 | 1.25E-09 |
| | hsa-let-7a-5p | | |
| Hippo signaling pathway | hsa-let-7a-5p | 52 | 4.10E-09 |
| | has-miR-181b-5p | | |
| Cell cycle | hsa-miR-222-3p | 47 | 2.22E-08 |
| | hsa-let-7a-5p | | |
| Viral carcinogenesis | hsa-let-7a-5p | 48 | 2.95E-07 |
| Oocyte meiosis | hsa-let-7a-5p | 35 | 4.06E-06 |
| Protein processing in endoplasmic reticulum | hsa-miR-222-3p | 37 | 4.08E-06 |
| | has-miR-181b-5p | | |
| Hepatitis B | hsa-let-7a-5p | 42 | 2.87E-05 |
| Adherents junction | hsa-let-7a-5p | 28 | 8.11E-05 |
| p53 signaling pathway | hsa-miR-222-3p | 33 | 0.00013438 |
| | has-miR-181b-5p | | |
| | hsa-let-7a-5p | | |
| Arrhythmogenic right ventricular cardiomyopathy (ARVC) | hsa-miR-222-3 | 16 | 0.00020225 |
| | phsa-let-7a-5p | | |
| Proteoglycans in cancer | hsa-let-7a-5p | 58 | 0.00039485 |
| | has-miR-181b-5p | | |
| ECM-receptor interaction | hsa-let-7a-5p | 15 | 0.00049296 |
| Ubiquitin mediated proteolysis | hsa-miR-222-3p | 53 | 0.00072422 |
| | has-miR-181b-5p | | |
| | hsa-let-7a-5p | | |
| Endocytosis | hsa-let-7a-5p | 45 | 0.0024329 |
| Thyroid hormone signaling pathway | hsa-let-7a-5p | 34 | 0.0026808 |
| Bacterial invasion of epithelial cells | hsa-let-7a-5p | 21 | 0.00606614 |
| HTLV-I infection | hsa-miR-222-3p | 64 | 0.01018435 |
| | hsa-let-7a-5p | | |
| TGF-beta signaling pathway | hsa-let-7a-5p | 27 | 0.01158769 |
| Pathways in cancer | hsa-let-7a-5p | 79 | 0.01428958 |
| Prostate cancer | has-miR-181b-5p | 13 | 0.0242868 |
| Transcriptional misregulation in cancer | hsa-let-7a-5p | 40 | 0.02522058 |
| Cell adhesion molecules (CAMs) | hsa-miR-222-3p | 9 | 0.02693923 |
| Chronic myeloid leukemia | hsa-let-7a-5p | 20 | 0.02993537 |
| Other types of O-glycan biosynthesis | hsa-let-7a-5p | 7 | 0.03647756 |
| Colorectal cancer | hsa-let-7a-5p | 15 | 0.04248994 |
| Renal cell carcinoma | has-miR-181b-5p | 10 | 0.04614817 |

miRPath DIANA v3.0 software was used to perform KEGG analysis using TarBase database. Pathways with a *p* < 0.05 was considered significant after false discovery rate correction.

cancer, miR-222 promotes chemotherapy resistance by targeting PTEN activating PI3K/AKT pathway [40]. Interestingly, miR181b sensitizes non-small cell lung cancer cells to chemotherapy by targeting directly TGFβR1/SMAD and indirectly PI3K/AKT pathway [41]. However, we did not find significant changes in expression levels of plasma sEV-packaged miR-181b-5p and miR-222-3p in non-IBC received neoadjuvant chemotherapy compared with untreated patients. Other PPI analysis has indicated that the tumor suppressor let-7a-5p is implicated in

various pathways that regulate apoptosis, cancer stem cell differentiation and inhibits cells invasion and proliferation of cancer cells [42–44]. Interestingly, in line with our KEGG analysis and its role in cell cycle, it was reported that let-7a targeted the HMGA1 gene responsible for proliferation of breast cancer cells and direct modulation of miR-181b expression which subsequently downregulates CBX7, a protein responsible for the cell cycle at G1 phase [45, 46]. Multiple lines of evidence demonstrated that overexpressed miR-181 induces cancer progression [47–49]. It is noteworthy that IBC tumor overexpress the heparan sulfate proteoglycan syndecan-1 [50], aligning with KEGG pathway analysis, including proteoglycans in cancer. In late stage breast cancer tissues, transient expression of miR-181b is activated by STAT3, a transcription factor activated by IL-6 [51], which results eventually in upregulation of NF-kB and downregulation of let-7a [52, 53]. This is consistent with the upregulated levels of miR-181b-5p in IBC relative to stage-matched non-IBC. Given the hyperactivation of STAT3, NF-kB and upregulated IL-6 expression in IBC [54], we propose the same mechanism of regulation may be found in IBC. Remarkably, a significant upregulation of exosomal miR-181b than that free in plasma was proven in lung cancer patients, suggesting that sEV-derived miRNAs could efficiently mirror the expression pattern of carcinoma tissues [55]. In agreement with our results, Wang *et al.* [56], showed that the target genes of miR222-3p are involved in viral infection, proteoglycans in cancer and transcriptional misregulation in cancer. Consistently, upregulated exosomal miR-222 was reported to downregulate PDLIM2 tumor suppressor and to activate NF-κB, which results in lymph node metastasis in advanced breast cancer [57]. Among the pathways in cancer indicated by KEGG analysis, the upregulated miR-222 was involved in pivotal pathways, such as OSM, IL-6 and ERK/MAPK signaling pathways in breast cancer [58], known pathways to be activated in IBC [59, 60]. The overexpression of miR-222 was verified in IBC tissues [34, 61] and potentially used in management of breast malignancy. Noticeably, exosomal miR-222-3p can serve as a prognostic marker for different cancers [62, 63]. Interestingly, human papillomavirus E6 and E7 oncoproteins potentiated tumorigenesis possibly via exosomal miR-222 [64], supporting the strong association of viral infection and IBC [65, 66]. The KEGG analysis showed that hub genes, which are the targets of miR-181b-5p, miR-222-3p and let-7a-5p were associated also to synapsis. Interestingly, it was demonstrated that the miRNAs analyzed actively participate in the normal maturation and development of the central nervous system and in Alzheimer disease [67–71]. Although the mechanism and the important players have not been described, patients with IBC have a high incidence of developing metastasis to the brain associated with a poor prognosis. These sEV-derived miRNAs (miR-181b-5p, miR-222-3p and let-7a-5p) and their target genes could probably be involved in the metastasis of the IBC to the brain [72–74], possibly via induction of formation of pre-metastatic niches [75, 76]. Indeed, it has been described that some miRNAs, such as miR-181 and let-7 and other exosomal miRNAs participate in metastasis to the brain of breast cancer cells [77, 78]. Furthermore, plasma EV- derived let-7a-5p may emerge as a predictive marker for the response to neoadjuvant chemotherapy, as it is the only miRNA whose expression level was affected by neoadjuvant chemotherapy. In agreement, a study reported an association of let-7a-5p expression with drug sensitivity in breast cancer cell lines [79], however this needs further investigation for confirmation in clinical setting. Finally, the identified miRNAs are involved in SNARE interactions, that are crucial for the fusion of multivesicular bodies with the plasma membrane during the release of sEVs [80]. Taken altogether, these sEV-derived miRNAs and their enrichment in signaling pathways not only implies their critical involvement in IBC development and progression, but also indicate that they may serve as more precise and stable biomarkers than free plasma miRNAs for metastatic IBC diagnosis. Besides, the 3-miRNA expression profile in IBC vs non-stage- and stage-matched comparisons with non-IBC further strongly suggests their specific expression pattern in enriched plasma sEVs of IBC.

The usage of sEV-derived miRNAs as potential diagnostic biomarkers has been examined in different tumor entities. For example, miR-181-5p discriminated between adenocarcinoma and squamous cell carcinoma of early-stage lung cancer [81]. Serum exosomes-derived miR-222 is a diagnostic marker for patients with high- and low-grade gliomas [82]. However, to our knowledge, no studies introduced EV-derived miRNA panels for IBC diagnosis. But different studies have introduced EV-derived miRNAs to differentiate breast cancer and healthy subjects [23, 83]. EV-derived miR-21 and miR-1246 with AUC of 0.73 and miR-142-5p and miR-320a with AUC of 0.941 fulfilled such purpose [23, 83]. We explored the diagnostic potential of the plasma sEV-encapsulated miR-222-3p, let-7a-5p and miR-181b-5p that may help in differentiation of IBC from non-IBC, either individually or combined. The estimated correlations between the three miRNAs indicate their combinative value. Using ROC curve analysis, the maximum AUC were reported for let-7a-5p (AUC = 0.919) and for combined (miR-222-3p and let-7a-5p) (AUC = 0.973), with considerably high discriminatory values for each. No change was noticed between AUC values of the three recombined miRNAs and the panel of miR-222 and let-7a. Thus, the later emerges as a more efficient, precise, and cost-effective biomarker than individual miRNA for IBC detection.

Although not tested in this study, one possible limitation is that the proposed method may not be applied for mass spectrometric analysis studies unless simple purification steps are added, such as column chromatography, size-exclusion, or potassium chloride precipitation [84, 85]. However, the exosomal proteome of Hela cells was successfully profiled by a PEG-based method [16], suggesting the potential of our optimized PEG-method to discover exosomes contained specific diagnostic proteomic IBC biomarkers.

## Conclusions

In summary, this study introduced DPEGT procedure as a minimally invasive PEG-based procedure for the isolation of sEVs from plasma biopsy as an alternative approach for the painful invasive tissue biopsy. Among the isolated miRNAs, three miRNAs (miR-181b-5p, miR-222-3p, and let-7a-5p) showed dysregulated miRNA expression levels consistently with their expression in IBC tissue carcinoma. The combined miR-222-3p and let-7a-5p showed excelled diagnostic potency for discriminating IBC from non-IBC patients. Further studies are warranted to decipher the influence of cargo of isolated sEVs on behavior of the cells within tumor microenvironmental cells, namely tumor-associated-macrophages and- fibroblasts, as well as their therapeutic potential needs further investigation.

## Supporting information

**S1 Fig. Dynamic Light Scattering (DLS) for sEV size distribution.** Comparison of sEV size distribution using different concentrations of (a) SPEGT and (b) DPEGT relative to ultracentrifugation and the miRCURY kit.
(TIF)

**S2 Fig. Gene stability of sEVs Reference Genes (RG).** RefFinder assigns values of gene stability for each candidate reference gene based on their geometric mean. Comparable geometric means ranging from 1.19 to 2.28 for cel-miR-39, miR-16 and RNU6.
(TIF)

**S3 Fig. Expression of miR-181b-5p, miR-222-3p and let-7a-5p from enriched plasma sEVs in non-IBC patients with stage I, II and III.** Relative expression levels of miR-181b-5p (a), miR-222-3p (b), and let-7a-5p (c) enriched in plasma sEVs of non-IBC patients with stage III (n = 10) and stage I or II (n = 24) by DPEGT. ns = not significant as determined by Student's

t-test.
(TIF)

**S4 Fig. Expression of miR-181b-5p, miR-222-3p and let-7a-5p from enriched plasma sEVs in neoadjuvant chemotherapy-treated and -untreated non-IBC patients.** Relative expression levels of miR-181b-5p (a), miR-222-3p (b), and let-7a-5p (c) enriched in plasma sEVs of non-IBC treated (n = 12) and untreated patients (n = 19) by DPEGT. $^{**}$ p < 0.01 and ns = not significant as determined by Student's t-test.
(TIF)

**S5 Fig. The network of miR-181b-5p, miR-222-3p, and let-7a-5p targets protein interactors.** String database output depicting functional and physical interactors of all targets from differentially regulated miRNAs.
(TIF)

**S6 Fig. Clustering and heat map of the KEGG enrichment pathways of miR-181b-5p, miR-222-3p, and let-7a-5p.** miRPath DIANA v3.0 software was used to generate the figure.
(TIF)

**S1 Table. All the modules obtained from MCODE analysis in Cytoscape are showed.** The most four significant modules (1–4), which contain the hub genes were selected. Later, these modules were submitted to String to find the KEGG pathways associated with these hub genes.
(XLSX)

**S1 Raw images.**
(ZIP)

## Author Contributions

**Conceptualization:** Martin Götte, Sherif Abdelaziz Ibrahim.

**Data curation:** Sarah Hamdy Ahmed, Nancy A. Espinoza-Sánchez, Ahmed El-Damen, Burkhard Greve, Martin Götte, Sherif Abdelaziz Ibrahim.

**Formal analysis:** Sarah Hamdy Ahmed, Ahmed El-Damen, Burkhard Greve, Martin Götte, Sherif Abdelaziz Ibrahim.

**Funding acquisition:** Sherif Abdelaziz Ibrahim.

**Investigation:** Sarah Hamdy Ahmed, Ahmed El-Damen, Martin Götte, Sherif Abdelaziz Ibrahim.

**Methodology:** Sarah Hamdy Ahmed, Ahmed El-Damen, Sherif Abdelaziz Ibrahim.

**Project administration:** Sherif Abdelaziz Ibrahim.

**Resources:** Mohamed El-Shinawi.

**Software:** Nancy A. Espinoza-Sánchez.

**Supervision:** Mohamed A. Badawy, Mohamed El-Shinawi, Sherif Abdelaziz Ibrahim.

**Writing – original draft:** Sarah Hamdy Ahmed, Sherif Abdelaziz Ibrahim.

**Writing – review & editing:** Sarah Hamdy Ahmed, Nancy A. Espinoza-Sánchez, Ahmed El-Damen, Sarah Atef Fahim, Burkhard Greve, Mohamed El-Shinawi, Martin Götte, Sherif Abdelaziz Ibrahim.

# References

1. Faldoni F. L. C., et al. "Inflammatory Breast Cancer: Clinical Implications of Genomic Alterations and Mutational Profiling," (in eng), *Cancers (Basel)*, vol. 12, no. 10, Sep 2020, https://doi.org/10.3390/cancers12102816 PMID: 33007869

2. Dobiasova B. and Mego M., "Biomarkers for Inflammatory Breast Cancer: Diagnostic and Therapeutic Utility," (in eng), *Breast Cancer (Dove Med Press)*, vol. 12, pp. 153–163, 2020, https://doi.org/10.2147/BCTT.S231502 PMID: 33116817

3. Soliman A. S., et al. "Inflammatory breast cancer in north Africa: comparison of clinical and molecular epidemiologic characteristics of patients from Egypt, Tunisia, and Morocco," (in eng), *Breast Dis*, vol. 33, no. 4, pp. 159–69, 2011–2012 2011, https://doi.org/10.3233/BD-2012-000337 PMID: 23001584

4. Diao J. D., et al. "Construction and validation of a nomogram to predict overall survival in patients with inflammatory breast cancer," (in eng), *Cancer Med*, vol. 8, no. 12, pp. 5600–5608, Sep 2019, https://doi.org/10.1002/cam4.2470 PMID: 31407527

5. Pan X., Yang W., Chen Y., Tong L., Li C., and Li H., "Nomogram for predicting the overall survival of patients with inflammatory breast cancer: A SEER-based study," (in eng), *Breast*, vol. 47, pp. 56–61, Oct 2019, https://doi.org/10.1016/j.breast.2019.05.015 PMID: 31351202

6. Dawood S., et al. "International expert panel on inflammatory breast cancer: consensus statement for standardized diagnosis and treatment," (in eng), *Ann Oncol*, vol. 22, no. 3, pp. 515–523, Mar 2011, https://doi.org/10.1093/annonc/mdq345 PMID: 20603440

7. Matsutani A., Udagawa C., Matsunaga Y., Nakamura S., and Zembutsu H., "Liquid biopsy for the detection of clinical biomarkers in early breast cancer: new insights and challenges," (in eng), *Pharmacogenomics*, vol. 21, no. 5, pp. 359–367, 04 2020, https://doi.org/10.2217/pgs-2019-0130 PMID: 32284011

8. Zha Q. B., Yao Y. F., Ren Z. J., Li X. J., and Tang J. H., "Extracellular vesicles: An overview of biogenesis, function, and role in breast cancer," (in eng), *Tumour Biol*, vol. 39, no. 2, p. 1010428317691182, Feb 2017, https://doi.org/10.1177/1010428317691182 PMID: 28231725

9. Yoshioka Y., N. C. C. R. I. Division of Molecular and Cellular Medicine, Tokyo, Japan, T. Katsuda, N. C. C. R. I. Division of Molecular and Cellular Medicine, Tokyo, Japan, T. Ochiya, and N. C. C. R. I. Division of Molecular and Cellular Medicine, Tokyo, Japan, "Extracellular vesicles and encapusulated miRNAs as emerging cancer biomarkers for novel liquid biopsy," *Japanese Journal of Clinical Oncology*, vol. 48, no. 10, pp. 869–876, 2020, https://doi.org/10.1093/jjco/hyy120 PMID: 30169666

10. Ibrahim S. A., Hassan H., and Götte M., "MicroRNA-dependent targeting of the extracellular matrix as a mechanism of regulating cell behavior," (in eng), *Biochim Biophys Acta*, vol. 1840, no. 8, pp. 2609–20, Aug 2014, https://doi.org/10.1016/j.bbagen.2014.01.022 PMID: 24462576

11. Liu Q., Peng F., and Chen J., "The Role of Exosomal MicroRNAs in the Tumor Microenvironment of Breast Cancer," (in eng), *Int J Mol Sci*, vol. 20, no. 16, Aug 2019, https://doi.org/10.3390/ijms20163884 PMID: 31395836

12. Lobb R. J., et al. "Optimized exosome isolation protocol for cell culture supernatant and human plasma," (in eng), *J Extracell Vesicles*, vol. 4, p. 27031, 2015, https://doi.org/10.3402/jev.v4.27031 PMID: 26194179

13. Konoshenko M. Y., Lekchnov E. A., Vlassov A. V., and Laktionov P. P., "Isolation of Extracellular Vesicles: General Methodologies and Latest Trends," (in eng), *Biomed Res Int*, vol. 2018, p. 8545347, 2018, https://doi.org/10.1155/2018/8545347 PMID: 29662902

14. Abramowicz A., Widlak P., and Pietrowska M., "Proteomic analysis of exosomal cargo: the challenge of high purity vesicle isolation," (in eng), *Mol Biosyst*, vol. 12, no. 5, pp. 1407–19, 04 2016, https://doi.org/10.1039/c6mb00082g PMID: 27030573

15. Rider M. A., Hurwitz S. N., and Meckes D. G., "ExtraPEG: A Polyethylene Glycol-Based Method for Enrichment of Extracellular Vesicles," (in eng), *Sci Rep*, vol. 6, p. 23978, Apr 2016, https://doi.org/10.1038/srep23978 PMID: 27068479

16. Weng Y., et al. "Effective isolation of exosomes with polyethylene glycol from cell culture supernatant for in-depth proteome profiling," (in en), 2016/05/04 2016, https://doi.org/10.1039/c6an00892e PMID: 27229443

17. Ludwig A. K., et al. "Precipitation with polyethylene glycol followed by washing and pelleting by ultracentrifugation enriches extracellular vesicles from tissue culture supernatants in small and large scales," (in eng), *J Extracell Vesicles*, vol. 7, no. 1, p. 1528109, 2018, https://doi.org/10.1080/20013078.2018.1528109 PMID: 30357008

18. Lv C., Ding W., Wang Y., Zhao Z., Li J., and Chen Y...., "A PEG-based method for the isolation of urinary exosomes and its application in renal fibrosis diagnostics using cargo miR-29c and miR-21 analysis," 2018. https://doi.org/10.1007/s11255-017-1779-4 PMID: 29330775

19. Kim J., Tan Z., and Lubman D. M., "Exosome enrichment of human serum using multiple cycles of centrifugation," (in eng), *Electrophoresis*, vol. 36, no. 17, pp. 2017–26, Sep 2015, https://doi.org/10.1002/elps.201500131 PMID: 26010067

20. Théry C., et al. "Minimal information for studies of extracellular vesicles 2018 (MISEV2018): a position statement of the International Society for Extracellular Vesicles and update of the MISEV2014 guidelines," (in en), https://doi.org/10.1080/20013078.2018.1535750, research-article 23 Nov 2018 2018, ZJEV-2018-0081.

21. Gardiner C., et al. "Measurement of refractive index by nanoparticle tracking analysis reveals heterogeneity in extracellular vesicles," (in eng), *J Extracell Vesicles*, vol. 3, p. 25361, 2014, https://doi.org/10.3402/jev.v3.25361 PMID: 25425324

22. M. L, et al. "Evaluation of circulating small extracellular vesicles derived miRNAs as biomarkers of early colon cancer: a comparison with plasma total miRNAs," *Journal of extracellular vesicles*, vol. 8, no. 1, 07/22/2019 2019, https://doi.org/10.1080/20013078.2019.1643670 PMID: 31448068

23. Hannafon B. N., et al. "Plasma exosome microRNAs are indicative of breast cancer," (in eng), *Breast Cancer Res*, vol. 18, no. 1, p. 90, 09 2016, https://doi.org/10.1186/s13058-016-0753-x PMID: 27608715

24. L. M, et al. "Circulating microRNAs from the miR-106a-363 cluster on chromosome X as novel diagnostic biomarkers for breast cancer," *Breast cancer research and treatment*, vol. 170, no. 2, 2018 Jul 2018, https://doi.org/10.1007/s10549-018-4757-3 PMID: 29557526

25. Rice J., Roberts H., Rai S. N., and Galandiuk S., "Housekeeping genes for studies of plasma microRNA: A need for more precise standardization," (in eng), *Surgery*, vol. 158, no. 5, pp. 1345–51, Nov 2015, https://doi.org/10.1016/j.surg.2015.04.025 PMID: 26094174

26. X. F, X. P, C. D, X. L, and Z. B, "miRDeepFinder: a miRNA analysis tool for deep sequencing of plant small RNAs," *Plant molecular biology*, 01/31/2012 2012, https://doi.org/10.1007/s11103-012-9885-2 PMID: 22290409

27. Vlachos I. S., et al. "DIANA-miRPath v3.0: deciphering microRNA function with experimental support," (in eng), *Nucleic Acids Res*, vol. 43, no. W1, pp. W460–6, Jul 2015, https://doi.org/10.1093/nar/gkv403 PMID: 25977294

28. Pathan M., et al. "FunRich: An open access standalone functional enrichment and interaction network analysis tool," (in eng), *Proteomics*, vol. 15, no. 15, pp. 2597–601, Aug 2015, https://doi.org/10.1002/pmic.201400515 PMID: 25921073

29. Pathan M., et al. "A novel community driven software for functional enrichment analysis of extracellular vesicles data," (in eng), *J Extracell Vesicles*, vol. 6, no. 1, p. 1321455, 2017, https://doi.org/10.1080/20013078.2017.1321455 PMID: 28717418

30. Huang d. W., Sherman B. T., and Lempicki R. A., "Bioinformatics enrichment tools: paths toward the comprehensive functional analysis of large gene lists," (in eng), *Nucleic Acids Res*, vol. 37, no. 1, pp. 1–13, Jan 2009, https://doi.org/10.1093/nar/gkn923 PMID: 19033363

31. Huang d. W., Sherman B. T, and Lempicki R. A., "Systematic and integrative analysis of large gene lists using DAVID bioinformatics resources," (in eng), *Nat Protoc*, vol. 4, no. 1, pp. 44–57, 2009, https://doi.org/10.1038/nprot.2008.211 PMID: 19131956

32. Szklarczyk D., et al. "STRING v11: protein-protein association networks with increased coverage, supporting functional discovery in genome-wide experimental datasets," (in eng), *Nucleic Acids Res*, vol. 47, no. D1, pp. D607–D613, 01 2019, https://doi.org/10.1093/nar/gky1131 PMID: 30476243

33. Shannon P., et al. "Cytoscape: a software environment for integrated models of biomolecular interaction networks," (in eng), *Genome Res*, vol. 13, no. 11, pp. 2498–504, Nov 2003, https://doi.org/10.1101/gr.1239303 PMID: 14597658

34. Fahim S. A., et al. "Inflammatory Breast Carcinoma: Elevated microRNA miR-181b-5p and Reduced miR-200b-3p, miR-200c-3p, and miR-203a-3p Expression as Potential Biomarkers with Diagnostic Value," (in eng), *Biomolecules*, vol. 10, no. 7, 07 2020, https://doi.org/10.3390/biom10071059 PMID: 32708601

35. Gandham S., et al. "Technologies and Standardization in Research on Extracellular Vesicles," (in eng), *Trends Biotechnol*, vol. 38, no. 10, pp. 1066–1098, 10 2020, https://doi.org/10.1016/j.tibtech.2020.05.012 PMID: 32564882

36. Mercadal M., et al. "Impact of Extracellular Vesicle Isolation Methods on Downstream Mirna Analysis in Semen: A Comparative Study," (in eng), *Int J Mol Sci*, vol. 21, no. 17, Aug 2020, https://doi.org/10.3390/ijms21175949 PMID: 32824915

37. Moon S., et al. "Enrichment of Exosome-Like Extracellular Vesicles from Plasma Suitable for Clinical Vesicular miRNA Biomarker Research," (in eng), *J Clin Med*, vol. 8, no. 11, Nov 2019, https://doi.org/10.3390/jcm8111995 PMID: 31731761

38. Morrow R. J., Etemadi N., Yeo B., and Ernst M., "Challenging a Misnomer? The Role of Inflammatory Pathways in Inflammatory Breast Cancer," (in en), *Mediators of Inflammation*, Review Article vol. 2017, 2017/05/21 2017, https://doi.org/10.1155/2017/4754827 PMID: 28607534

39. Ihle M. A., et al. "miRNA-221 and miRNA-222 induce apoptosis via the KIT/AKT signalling pathway in gastrointestinal stromal tumours," *Mol Oncol*, vol. 9, no. 7, pp. 1421–33, Aug 2015, https://doi.org/10.1016/j.molonc.2015.03.013 PMID: 25898773

40. Amini-Farsani Z., Sangtarash M. H., Shamsara M., and Teimori H., "MiR-221/222 promote chemoresistance to cisplatin in ovarian cancer cells by targeting PTEN/PI3K/AKT signaling pathway," (in eng), *Cytotechnology*, vol. 70, no. 1, pp. 203–213, Feb 2018, https://doi.org/10.1007/s10616-017-0134-z PMID: 28887606

41. Wang X., et al. "MiR-181b regulates cisplatin chemosensitivity and metastasis by targeting TGFβR1/Smad signaling pathway in NSCLC," (in eng), *Sci Rep*, vol. 5, p. 17618, Dec 2015, https://doi.org/10.1038/srep17618 PMID: 26620926

42. Yin P. T., et al. "Overcoming Chemoresistance in Cancer via Combined MicroRNA Therapeutics with Anticancer Drugs Using Multifunctional Magnetic Core-Shell Nanoparticles," (in eng), *ACS Appl Mater Interfaces*, vol. 10, no. 32, pp. 26954–26963, Aug 2018, https://doi.org/10.1021/acsami.8b09086 PMID: 30028120

43. Barh D., Malhotra R., Ravi B., and Sindhurani P., "MicroRNA let-7: an emerging next-generation cancer therapeutic," (in eng), *Curr Oncol*, vol. 17, no. 1, pp. 70–80, Feb 2010, https://doi.org/10.3747/co.v17i1.356 PMID: 20179807

44. Xu C., et al. "Let-7a regulates mammosphere formation capacity through Ras/NF-κB and Ras/MAPK/ERK pathway in breast cancer stem cells," (in eng), *Cell Cycle*, vol. 14, no. 11, pp. 1686–97, 2015, https://doi.org/10.1080/15384101.2015.1030547 PMID: 25955298

45. Mansueto G., et al. "Identification of a New Pathway for Tumor Progression: MicroRNA-181b Up-Regulation and CBX7 Down-Regulation by HMGA1 Protein," (in eng), *Genes Cancer*, vol. 1, no. 3, pp. 210–24, Mar 2010, https://doi.org/10.1177/1947601910366860 PMID: 21779448

46. Liu K., et al. "Let-7a inhibits growth and migration of breast cancer cells by targeting HMGA1," (in eng), *Int J Oncol*, vol. 46, no. 6, pp. 2526–34, 2015, https://doi.org/10.3892/ijo.2015.2949 PMID: 25846193

47. Strotbek M., Schmid S., Sánchez-González I., Boerries M., Busch H., and Olayioye M. A., "miR-181 elevates Akt signaling by co-targeting PHLPP2 and INPP4B phosphatases in luminal breast cancer," (in eng), *Int J Cancer*, vol. 140, no. 10, pp. 2310–2320, 05 2017, https://doi.org/10.1002/ijc.30661 PMID: 28224609

48. Bisso A., et al. "Oncogenic miR-181a/b affect the DNA damage response in aggressive breast cancer," (in eng), *Cell Cycle*, vol. 12, no. 11, pp. 1679–87, Jun 2013, https://doi.org/10.4161/cc.24757 PMID: 23656790

49. Zheng Y., et al. "MiR-181b promotes chemoresistance in breast cancer by regulating Bim expression," *Oncol Rep*, vol. 35, no. 2, pp. 683–90, Feb 2016, https://doi.org/10.3892/or.2015.4417 PMID: 26572075

50. SA I., et al. "Syndecan-1 is a novel molecular marker for triple negative inflammatory breast cancer and modulates the cancer stem cell phenotype via the IL-6/STAT3, Notch and EGFR signaling pathways," *Molecular cancer*, vol. 16, no. 1, 03/07/2017 2017, https://doi.org/10.1186/s12943-017-0621-z PMID: 28270211

51. Andalib A., Rashed S., Dehbashi M., Hajati J., Noorbakhsh F., and Ganjalikhani-Hakemi M., "The Upregulation of hsa-mir-181b-1 and Downregulation of Its Target CYLD in the Late-Stage of Tumor Progression of Breast Cancer," (in eng), *Indian J Clin Biochem*, vol. 35, no. 3, pp. 312–321, Jul 2020, https://doi.org/10.1007/s12291-019-00826-z PMID: 32647409

52. Iliopoulos D., Jaeger S. A., Hirsch H. A., Bulyk M. L., and Struhl K., "STAT3 activation of miR-21 and miR-181b-1 via PTEN and CYLD are part of the epigenetic switch linking inflammation to cancer," (in eng), *Mol Cell*, vol. 39, no. 4, pp. 493–506, Aug 2010, https://doi.org/10.1016/j.molcel.2010.07.023 PMID: 20797623

53. Iliopoulos D., Hirsch H. A., and Struhl K., "An epigenetic switch involving NF-kappaB, Lin28, Let-7 MicroRNA, and IL6 links inflammation to cell transformation," (in eng), *Cell*, vol. 139, no. 4, pp. 693–706, Nov 2009, https://doi.org/10.1016/j.cell.2009.10.014 PMID: 19878981

54. Wang X., et al. "Targeting Signaling Pathways in Inflammatory Breast Cancer," (in eng), *Cancers (Basel)*, vol. 12, no. 9, Sep 2020, https://doi.org/10.3390/cancers12092479 PMID: 32883032

55. Tian F., Shen Y., Chen Z., Li R., and Ge Q., "No Significant Difference between Plasma miRNAs and Plasma-Derived Exosomal miRNAs from Healthy People," (in eng), *Biomed Res Int*, vol. 2017, p. 1304816, 2017, https://doi.org/10.1155/2017/1304816 PMID: 28656135

56. Wang X., et al. "Clustered microRNAs hsa-miR-221-3p/hsa-miR-222-3p and their targeted genes might be prognostic predictors for hepatocellular carcinoma," *J Cancer*, vol. 10, no. 11, pp. 2520–2533, 2019, https://doi.org/10.7150/jca.29207 PMID: 31258758

57. D. J, et al. "Exosome-mediated miR-222 transferring: An insight into NF-κB-mediated breast cancer metastasis," *Experimental cell research*, vol. 369, no. 1, 08/01/2018 2018, https://doi.org/10.1016/j.yexcr.2018.05.014 PMID: 29778754

58. Bottai G., et al. "Integrated MicroRNA-mRNA Profiling Identifies Oncostatin M as a Marker of Mesenchymal-Like ER-Negative/HER2-Negative Breast Cancer," (in eng), *Int J Mol Sci*, vol. 18, no. 1, Jan 2017, https://doi.org/10.3390/ijms18010194 PMID: 28106823

59. Iwase T., et al. "Quantitative hormone receptor (HR) expression and gene expression analysis in HR+ inflammatory breast cancer (IBC) vs non-IBC," (in eng), *BMC Cancer*, vol. 20, no. 1, p. 430, May 2020, https://doi.org/10.1186/s12885-020-06940-z PMID: 32423453

60. Lim B., Woodward W. A., Wang X., Reuben J. M., and Ueno N. T., "Author Correction: Inflammatory breast cancer biology: the tumour microenvironment is key," (in eng), *Nat Rev Cancer*, vol. 18, no. 8, p. 526, Aug 2018, https://doi.org/10.1038/s41568-018-0022-7 PMID: 29748602

61. Lerebours F., et al. "miRNA expression profiling of inflammatory breast cancer identifies a 5-miRNA signature predictive of breast tumor aggressiveness," *International journal of cancer. Journal international du cancer*, vol. 133, no. 7, pp. 1614–23, Oct 1 2013, https://doi.org/10.1002/ijc.28171 PMID: 23526361

62. Wei F., et al. "Exosomes derived from gemcitabine-resistant cells transfer malignant phenotypic traits via delivery of miRNA-222-3p," (in eng), *Mol Cancer*, vol. 16, no. 1, p. 132, 07 2017, https://doi.org/10.1186/s12943-017-0694-8 PMID: 28743280

63. Li Z., et al. "Tumor-Secreted Exosomal miR-222 Promotes Tumor Progression via Regulating P27 Expression and Re-Localization in Pancreatic Cancer," (in eng), *Cell Physiol Biochem*, vol. 51, no. 2, pp. 610–629, 2018, https://doi.org/10.1159/000495281 PMID: 30458449

64. MV C., et al. "Human papillomavirus E6 and E7 oncoproteins affect the expression of cancer-related microRNAs: additional evidence in HPV-induced tumorigenesis," *Journal of cancer research and clinical oncology*, vol. 142, no. 8, 2016 Aug 2016, https://doi.org/10.1007/s00432-016-2189-1 PMID: 27300513

65. E.-S. M, et al. "Inflammatory and Non-inflammatory Breast Cancer: A Potential Role for Detection of Multiple Viral DNAs in Disease Progression," *Annals of surgical oncology*, vol. 23, no. 2, 2016 Feb 2016, https://doi.org/10.1245/s10434-015-4888-2 PMID: 26508152

66. C. M, et al. "Prevalence of papillomaviruses, polyomaviruses, and herpesviruses in triple-negative and inflammatory breast tumors from algeria compared with other types of breast cancer tumors," *PloS one*, vol. 9, no. 12, 12/05/2014 2014, https://doi.org/10.1371/journal.pone.0114559 PMID: 25478862

67. Fairchild C. L. A., Cheema S. K., Wong J., Hino K., Simo S., and La Torre A., "Let-7 regulates cell cycle dynamics in the developing cerebral cortex and retina," *Sci Rep*, vol. 9, no. 1, p. 15336, Oct 25 2019, https://doi.org/10.1038/s41598-019-51703-x PMID: 31653921

68. Kapsimali M., Kloosterman W. P., de Bruijn E., Rosa F., Plasterk R. H., and Wilson S. W., "MicroRNAs show a wide diversity of expression profiles in the developing and mature central nervous system," *Genome Biol*, vol. 8, no. 8, p. R173, 2007, https://doi.org/10.1186/gb-2007-8-8-r173 PMID: 17711588

69. Kos A., et al. "MicroRNA-181 promotes synaptogenesis and attenuates axonal outgrowth in cortical neurons," *Cell Mol Life Sci*, vol. 73, no. 18, pp. 3555–67, Sep 2016, https://doi.org/10.1007/s00018-016-2179-0 PMID: 27017280

70. Rodriguez-Ortiz C. J., et al. "miR-181a negatively modulates synaptic plasticity in hippocampal cultures and its inhibition rescues memory deficits in a mouse model of Alzheimer's disease," *Aging Cell*, vol. 19, no. 3, p. e13118, Mar 2020, https://doi.org/10.1111/acel.13118 PMID: 32087004

71. Catana C. S., Crisan C. A., Opre D., and Berindan-Neagoe I., "Diagnostic and prognostic value of microRNAs for Alzheimer's disease: a comprehensive meta-analysis," *Med Pharm Rep*, vol. 93, no. 1, pp. 53–61, Jan 2020, https://doi.org/10.15386/mpr-1393 PMID: 32133447

72. Warren L. E., et al. "Inflammatory breast cancer and development of brain metastases: risk factors and outcomes," *Breast Cancer Res Treat*, vol. 151, no. 1, pp. 225–32, May 2015, https://doi.org/10.1007/s10549-015-3381-8 PMID: 25893587

73. Dawood S., et al. "Incidence of and survival following brain metastases among women with inflammatory breast cancer," *Ann Oncol*, vol. 21, no. 12, pp. 2348–2355, Dec 2010, https://doi.org/10.1093/annonc/mdq239 PMID: 20439340

74. Uemura M. I., et al. "Development of CNS metastases and survival in patients with inflammatory breast cancer," *Cancer*, vol. 124, no. 11, pp. 2299–2305, Jun 1 2018, https://doi.org/10.1002/cncr.31336 PMID: 29579338

75. Guo Y., et al. "Effects of exosomes on pre-metastatic niche formation in tumors," *Mol Cancer*, vol. 18, no. 1, p. 39, Mar 11 2019, https://doi.org/10.1186/s12943-019-0995-1 PMID: 30857545

76. Hoshino A., et al. "Tumour exosome integrins determine organotropic metastasis," *Nature*, vol. 527, no. 7578, pp. 329–35, Nov 19 2015, https://doi.org/10.1038/nature15756 PMID: 26524530

77. Kanchan R. K., Siddiqui J. A., Mahapatra S., Batra S. K., and Nasser M. W., "microRNAs Orchestrate Pathophysiology of Breast Cancer Brain Metastasis: Advances in Therapy," *Mol Cancer*, vol. 19, no. 1, p. 29, Feb 15 2020, https://doi.org/10.1186/s12943-020-1140-x PMID: 32059676

78. Wong G. L., Abu Jalboush S., and Lo H. W., "Exosomal MicroRNAs and Organotropism in Breast Cancer Metastasis," *Cancers (Basel)*, vol. 12, no. 7, Jul 7 2020, https://doi.org/10.3390/cancers12071827 PMID: 32646059

79. Uhr K., et al. "MicroRNAs as possible indicators of drug sensitivity in breast cancer cell lines," (in eng), *PLoS One*, vol. 14, no. 5, p. e0216400, 2019, https://doi.org/10.1371/journal.pone.0216400 PMID: 31063487

80. Mills J., Capece M., Cocucci E., Tessari A., and Palmieri D., "Cancer-Derived Extracellular Vesicle-Associated MicroRNAs in Intercellular Communication: One Cell's Trash Is Another Cell's Treasure," *Int J Mol Sci*, vol. 20, no. 24, Dec 4 2019, https://doi.org/10.3390/ijms20246109 PMID: 31817101

81. Jin X., et al. "Evaluation of Tumor-Derived Exosomal miRNA as Potential Diagnostic Biomarkers for Early-Stage Non-Small Cell Lung Cancer Using Next-Generation Sequencing," (in eng), *Clin Cancer Res*, vol. 23, no. 17, pp. 5311–5319, Sep 2017, https://doi.org/10.1158/1078-0432.CCR-17-0577 PMID: 28606918

82. Santangelo A., et al. "A microRNA signature from serum exosomes of patients with glioma as complementary diagnostic biomarker," (in eng), *J Neurooncol*, vol. 136, no. 1, pp. 51–62, Jan 2018, https://doi.org/10.1007/s11060-017-2639-x PMID: 29076001

83. Ozawa P. M. M., et al. "Identification of miRNAs Enriched in Extracellular Vesicles Derived from Serum Samples of Breast Cancer Patients," (in eng), *Biomolecules*, vol. 10, no. 1, 01 2020, https://doi.org/10.3390/biom10010150 PMID: 31963351

84. L. K, R. KJ, and S. LA, "Preparing lambda DNA from phage lysates," *Current protocols in molecular biology*, vol. Chapter 1, 2001 May 2001, https://doi.org/10.1002/0471142727.mb0113s10 PMID: 18265041

85. KR Y., BM A., B. R, L. L, and T. G, "Rapid bacteriophage sedimentation in the presence of polyethylene glycol and its application to large-scale virus purification," *Virology*, vol. 40, no. 3, 1970 Mar 1970, https://doi.org/10.1016/0042-6822(70)90218-7